Universität Stuttgart

Fachbereich Mathematik

Relaxed Navier-Stokes-Korteweg Equations for Compressible Two-Phase Flow with Phase Transition

Jochen Neusser, Christian Rohde, Veronika Schleper

Preprint 2014/021

Fachbereich Mathematik
Fakultät Mathematik und Physik
Universität Stuttgart
Pfaffenwaldring 57
D-70 569 Stuttgart

E-Mail: preprints@mathematik.uni-stuttgart.de
WWW: http://www.mathematik.uni-stuttgart.de/preprints

ISSN **1613-8309**

Relaxed Navier-Stokes-Korteweg Equations for Compressible Two-Phase Flow with Phase Transition

Jochen Neusser*, Christian Rohde, Veronika Schleper

Universität Stuttgart, Institut für Angewandte Analysis und Numerische Simulation, Pfaffenwaldring 57, D-70569 Stuttgart, Germany,
jochen.neusser|crohde|veronika.schleper@mathematik.uni-stuttgart.de

SUMMARY

The Navier-Stokes-Korteweg (NSK) system is a classical diffuse-interface model for compressible two-phase flow. However, the direct numerical simulation based on the NSK system is quite expensive and in some cases even not possible.
We propose a relaxed lower-order approximation of the NSK system with hyperbolic first-order part. This allows to apply numerical methods for hyperbolic conservation laws and to remove some of the difficulties of the original NSK system. To illustrate the new ansatz we first present a 1D solver based Local-Discontinuous-Galerkin method in one and two spatial dimensions. It is shown that we can compute initial-boundary-value problems with realistic density ratios, and to perform stable computations for small interfacial widths. As a second application we show that it is possible to construct a semi-discrete finite-difference scheme which satisfies a discrete entropy inequality.

Submitted . . .

KEY WORDS: Diffuse-Interface Model, Compressible Flow with Phase Transition, Discrete Thermodynamical Consistency

1. INTRODUCTION

For the mathematical description of the dynamics of a two-phase fluid one can rely either on a sharp-interface (SI) or a diffuse-interface (DI) approach. For the latter model concept the phase boundary is artificially smeared out over a small interfacial region such that only one set of equations is used in the complete spatial domain. In contrast to the discretization methods for sharp-interface models those for diffuse interface models are not faced with the difficulty to track the interface explicitly as a free boundary. Therefore DI models provide a promising tool for the direct numerical simulation of e.g. the merging process of single droplets or bubbles.

We consider in this paper a class of DI models for a homogeneous compressible fluid that can appear in a vapour and in a liquid phase allowing for phase transition. While DI models are attractive because they can govern fluid flow with topological changes it turns out that it is not a straightforward task to construct DI models that take into account properly capillarity effects, *and*

*Correspondence to: Jochen Neusser

at the same time obey the second law of thermodynamics. The oldest approach to DI modelling for compressible flow can be traced back to a work of Korteweg [28]. His ideas have been taken up by Dunn&Serrin [18] (see also [2]) to formulate the by now classical Navier-Stokes-Korteweg (NSK) system. Formally the NSK system is a third-order extension of the Navier-Stokes equations using a Van-der-Waals like pressure function which is nonmonotone with respect to density, and thus allows the identification of two distinct phases. For the NSK system and its variants various analytical well-posedness results have been achieved in the last twenty years which justify this model. We refer to [4, 7, 25, 29, 33], to mention just a few. Also the topic of numerically solving the NSK system has been discussed by many authors, e.g. [6, 13, 16, 22, 24, 27, 39]. Despite these efforts there are still severe open problems for the numerical treatment. Up to our knowledge no numerical schemes have been suggested that allow the robust computation of problems with realistic density values for liquid and vapour phases. We recall that e.g., the densities of vapour and liquid water at $T = 20°C$ differ by a factor of 10^5. Moreover discretization methods fail also for very tiny interfacial widths close to a sharp interface. Both problems are related to the occurence of steep density gradients within the solution. Note that the Van-der-Waals like form of the pressure excludes the use of upwind hyperbolic solvers which have been applied successfully to stabilize computations for high Reynolds number Navier-Stokes computations. In particular the issue of tiny interfaces is of highest importance since it has been shown that the NSK model can only provide the correct amount of capillary force if the interface is extremely small [17, 26, 27]. These considerations motivated researchers to construct models which loosen the coupling between interfacial width and capillarity forces. The standard ansatz is to introduce an additional Allen-Cahn or Cahn-Hilliard type equation for a new explicit phase-field variable. We refer to [5] and the more recent works [1, 40]. The numerics for the explicit phase-field models is still in the very beginning.

The present paper relies on the older NSK ideas. To avoid (at least some of) the aforementioned difficulties for the classical NSK system we will suggest nonlocal relaxed NSK systems (which have already been considered for analytical purposes in [34]). These models are parametrized by a so-called Korteweg parameter. If the Korteweg parameter tends to infinity the classical NSK system is formally recovered such that the relaxed version can be seen as an approximation. On the other hand the relaxed system has its own importance for a fixed positive Korteweg parameter. It is of lower order but contains an additional elliptic constraint in the form of a screened Poisson equation. We will show that the relaxed system is in accordance with the second law of thermodynamics and comment on the effective amount of capillarity. The relaxed model formulations and its main properties are introduced in Section 2, together with the basic thermodynamical framework.

The most important feature of the relaxed system is the fact that the first-order part is *purely hyperbolic* for sufficiently large Korteweg parameter. It is the main purpose of this contribution to show how this property can be used to construct efficient and robust numerical schemes.

In the first numerical Section 3 we exploit the hyperbolic structure of the model and construct Local-Discontinuous-Galerkin (LDG) methods for the relaxed system. The ansatz combines in

particular the LDG ideas and Riemann solvers for the hydrodynamical part [3, 10, 11, 12] with LDG discretizations for elliptic equations [31]. For the sake of comparison also an LDG discretization of the classical NSK system is given in detail.
We will show then in Section 4 that the algorithm for the relaxed NSK system is robust for

(a) problems with large density ratios,
(b) problems with small interfacial widths.

To show that the model and the scheme are able to reproduce interesting phase transition flows we present twodimensional simulations for the merging of bubbles.
In the second numerical Section 5 we construct a simple semi-discrete finite-volume scheme for the relaxed NSK system that can be proven to obey the second law of thermodynamics on the discrete level. We note that this kind of entropy stability is usually seen as a guideline in the design of numerical methods. Our method relies essentially on the formulation of entropy-conservative schemes as they have been introduced by Tadmor [37, 38] for first-order hyperbolic systems. Up to our knowledge a comparable approach has not been found for the original NSK system. Methods to enforce entropy stability there typically introduce quite complex stabilization mechanisms (see e.g. [6, 24, 22]).

2. LIQUID-VAPOUR FLUIDS AND NAVIER-STOKES-KORTEWEG MODELLING

2.1. Liquid-Vapour Fluids

We consider the isothermal situation at some fixed temperature $T_* > 0$, such that the thermodynamical quantities depend only on density $\rho \in (0, b)$, $b > 0$. Let a free energy function $W : (0, b) \to (0, \infty)$ be given. For us the Van-der-Waals case will serve as a prototype, where W is defined by

$$W(\rho) = \frac{RT_*}{b}\rho \ln\left(\frac{\rho}{b-\rho}\right) - a\rho^2 + \rho g(T_*). \tag{1}$$

Thereby a and R are positive constants and $g = g(T_*)$ is a function of temperature alone.
From the energy expression (1) the pressure $p : (0, b) \to (0, \infty)$ is derived by

$$p(\rho) = \rho W'(\rho) - W(\rho), \tag{2}$$

which results for the choice (1) in

$$p(\rho) = \frac{RT_*\rho}{b-\rho} - a\rho^2. \tag{3}$$

To describe a two-phase fluid the constant reference temperature T_* is chosen so small such that W is concave in some non-empty density interval (r_1, r_2). Since (2) implies the relation $p'(\rho) = \rho W''(\rho)$ we observe that p is monotone decreasing in (r_1, r_2). This structure allows to define phases. If the density ρ lies in the interval $(0, r_1]$, $((r_1, r_2))$, $\{[r_2, b)\}$ the corresponding fluid state is called *vapour (spinodal)* $\{$*liquid*$\}$. We refer to Figure 1 for some illustration and note that we will use throughout

the paper the choice

$$a = 3, \qquad b = 3, \qquad T_* = 0.85, \qquad R = 8. \tag{4}$$

This implies

$$r_1 \approx 0.5811, \qquad r_2 \approx 1.4888. \tag{5}$$

The function g in (1) is not specified since it plays no role in the isothermal setting.

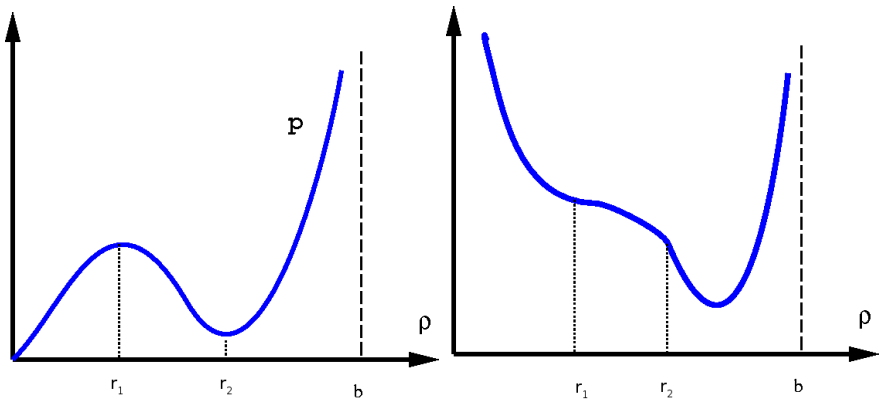

Figure 1. Graph of the pressure p and the free energy W.

2.2. *The Euler and the Navier-Stokes-Korteweg System*

We proceed to describe the dynamics of a liquid-vapour fluid in some open set $\Omega \subseteq \mathbb{R}^d$, $d \in \{1, 2, 3\}$, up to the end time $T > 0$. Let us first neglect viscosity and capillary effects. With the unknowns density $\rho = \rho(\mathbf{x}, t) \in (0, b)$ and velocity $\mathbf{v} = \mathbf{v}(\mathbf{x}, t) = (v_1(\mathbf{x}, t), \cdots, v_d(\mathbf{x}, t))^T \in \mathbb{R}^d$ the ideal dynamics is given by

$$\begin{aligned} \rho_t &+ \operatorname{div}(\rho \mathbf{v}) &&= 0 \\ (\rho \mathbf{v})_t &+ \operatorname{div}(\rho \mathbf{v}\mathbf{v}^T + p(\rho)\mathbf{I}) &&= 0 \end{aligned} \qquad \text{in } \Omega_T := \Omega \times (0, T). \tag{6}$$

Here $\mathbf{I} \in \mathbb{R}^{d \times d}$ denotes the unity matrix.

Taking $d = 2$ for simplicity, the system (6) in conservative form is rewritten as

$$\mathbf{u}_t + \mathbf{f}^1(\mathbf{u})_{x_1} + \mathbf{f}^2(\mathbf{u})_{x_2} = 0 \tag{7}$$

with state vector $\mathbf{u} = (\rho, m_1, m_2)^T = (\rho, \rho v_1, \rho v_2)^T$ and $\mathbf{f}^{1/2} = \mathbf{f}^{1/2}(\mathbf{u})$ defined by

$$\mathbf{f}^1(\mathbf{u}) = \left(\rho v_1, \rho v_1^2 + p(\rho), \rho v_1 v_2\right)^T, \qquad \mathbf{f}^2(\mathbf{u}) = \left(\rho v_2, \rho v_1 v_2, \rho v_2^2 + p(\rho)\right)^T.$$

The eigenvalues of the Jacobian $n_1 D\mathbf{f}^1(\mathbf{u}) + n_2 D\mathbf{f}^2(\mathbf{u}) \in \mathbb{R}^{3\times 3}$ for some vector $\mathbf{n} = (n_1, n_2)^T \in \mathcal{S}^1$ are then

$$\lambda_1(\mathbf{u}) = \mathbf{v} \cdot \mathbf{n} - \sqrt{p'(\rho)}, \qquad \lambda_2(\mathbf{u}) = \mathbf{v} \cdot \mathbf{n}, \qquad \lambda_3(\mathbf{u}) = \mathbf{v} \cdot \mathbf{n} + \sqrt{p'(\rho)} \tag{8}$$

with corresponding eigenvectors

$$\mathbf{K}_1(\mathbf{u}) = \begin{pmatrix} 1 \\ v_1 - n_1\sqrt{p'(\rho)} \\ v_2 - n_2\sqrt{p'(\rho)} \end{pmatrix}, \quad \mathbf{K}_1(\mathbf{u}) = \begin{pmatrix} 0 \\ n_2 \\ -n_1 \end{pmatrix}, \quad \mathbf{K}_3(\mathbf{u}) = \begin{pmatrix} 1 \\ v_1 + n_1\sqrt{p'(\rho)} \\ v_2 + n_2\sqrt{p'(\rho)} \end{pmatrix}. \tag{9}$$

We observe that (7) is not purely hyperbolic for all density values. In view of a two-phase pressure (3) it is hyperbolic if and only if the density is in bulk phases, i.e., for $\rho \in (0,b) \setminus [r_1, r_2]$. The same applies for the general model (6) which is hyperbolic in the state space $\mathcal{U} := \big((0,r_1) \cup (r_2,b)\big) \times \mathbb{R}^d$. $\mathcal{U}$ is obviously non-convex.

This failure of hyperbolicity (and the necessity to impose coupling conditions like the Young-Laplace relation explicitly on the fluid interface) requires to include complex tracking mechanisms into discretization methods. Thus diffuse-interface models appear to be promising alternative approaches. The classical approach consists of the Naviers-Stokes-Korteweg(NSK) system [2, 18], which is given by

$$\begin{aligned} \rho^\varepsilon_t &+ \operatorname{div}(\rho^\varepsilon \mathbf{v}^\varepsilon) &&= 0 \\ (\rho^\varepsilon \mathbf{v}^\varepsilon)_t &+ \operatorname{div}(\rho^\varepsilon \mathbf{v}^\varepsilon \otimes \mathbf{v}^\varepsilon + p(\rho^\varepsilon)\mathbf{I}) &&= \operatorname{div}(\mathbf{T}^\varepsilon[\mathbf{v}^\varepsilon]) + \gamma\varepsilon^2 \rho^\varepsilon \nabla\Delta\rho^\varepsilon \end{aligned} \quad \text{in } \Omega_T. \tag{10}$$

The matrix $\mathbf{T}^\varepsilon[\mathbf{v}] \in \mathbb{R}^{d\times d}$ in (10) stands for the viscous part of the stress tensor which is given for $\lambda, \mu \in \mathbb{R}$ with $\mu \geq 0$ and $3\lambda + 2\mu > 0$ by

$$\mathbf{T}^\varepsilon_{ij} := \varepsilon\lambda \operatorname{div}(\mathbf{v})\delta_{ij} + 2\varepsilon\mu \mathbf{D}_{ij}, \qquad \mathbf{D}_{ij} := \frac{1}{2}\Big(v_{j,x_i} + v_{i,x_j}\Big) \qquad (i,j \in \{1,2\}). \tag{11}$$

The parameters $\varepsilon, \gamma > 0$ in (10) tune the width of the diffuse interface and the effective surface tension (cf. Remark 2.2 below). For the *sharp-interface limit* $\varepsilon \to 0$ we expect that a sequence of solutions $\{(\rho^\varepsilon, \mathbf{v}^\varepsilon)\}_{\varepsilon>0}$ of some initial-boundary value problem for (10) converges to a weak solution of the associated problem for (6).

Proposition 2.1. For $\rho_0 : \Omega \to (0,b)$ and $\mathbf{v}_0 : \Omega \to \mathbb{R}^d$ let $(\rho^\varepsilon, \mathbf{v}^\varepsilon)$ be a classical solution of (10) which satisfies the initial conditions

$$\rho^\varepsilon(\cdot,0) = \rho_0, \ \mathbf{v}^\varepsilon(\cdot,0) = \mathbf{v}_0 \text{ in } \Omega \tag{12}$$

and the boundary conditions

$$\mathbf{v}^\varepsilon = 0, \ \nabla\rho^\varepsilon \cdot \mathbf{n} = 0 \text{ in } \partial\Omega, \tag{13}$$

where $\mathbf{n}$ denotes the (outer) normal vector associated with $\partial\Omega$.
Then we have for $t \in [0,T)$

$$\begin{aligned} &\mathcal{E}^\varepsilon[\rho^\varepsilon(\cdot,t), \mathbf{v}^\varepsilon(\cdot,t)] - \mathcal{E}^\varepsilon[\rho_0, \mathbf{v}_0] \\ &\qquad = -\varepsilon \int_0^t \int_\Omega 2\mu \mathbf{D}(\mathbf{v}^\varepsilon(\mathbf{x},s)) : \mathbf{D}(\mathbf{v}^\varepsilon(\mathbf{x},s)) + \lambda(\operatorname{div}(\mathbf{v}^\varepsilon(\mathbf{x},s)))^2 \, d\mathbf{x}ds. \end{aligned} \tag{14}$$

In (14) we used the van-der-Waals energy

$$\mathcal{E}^\varepsilon[\rho, \mathbf{v}] = \int_\Omega \left(\frac{1}{2}\rho(\mathbf{x})|\mathbf{v}(\mathbf{x})|^2 + W(\rho(\mathbf{x})) + \gamma\varepsilon^2 \frac{|\nabla\rho(\mathbf{x})|^2}{2} \right) d\mathbf{x}. \tag{15}$$

Proof

cf. [2, 34]. □

The expression $\mathcal{E}^\varepsilon[\rho, \mathbf{v}]$ is the natural total energy term for the NSK system including kinetic, potential and interfacial energy. Proposition 2.1 ensures the thermodynamical consistency of the NSK system (10). Analytical results on the wellposedness of initial-boundary problems for (10) that rely essentially on the energy estimate (14) can be found in [7, 25].

The numerical solution of (10) becomes quite intricate and expensive due to the third-order derivative in the momentum balance and the lack of hyperbolicity in the first-order part of (10) as discussed above. Note that the latter is exactly given by (6). Explicit schemes suffer from extremely small time steps while implicit discretizations lead to badly conditioned algebraic problems. The non-monotonicity of p prevents the use of most modern shock-capturing schemes. As a consequence it is almost impossible to perform numerical simulations in the sharp-interface limit or for realistic variations of the density.

Remark 2.2. (i) Note that the choice (13) of the boundary condition for ρ^ε leads to a 90^o degree contact angle between the phases at the boundary.

(ii) Various authors have pointed out that the parameter $\varepsilon > 0$ does not only control the interfacial width but also the effective surface tension of solutions for (10) [17, 26, 27]. Since surface tension is prescribed by the fluid under consideration the parameter ε is prescribed and cannot be tuned to enlarge e.g. the interface for numerical reasons. Moreover a dimensional analysis shows that realistic surface tension values can imply that ε has to be chosen so small such that a numerical resolution of the interface cannot be realized.

2.3. A Relaxed Navier-Stokes-Korteweg System

Having in mind the shortcomings of the classical NSK system we suggest in this section a relaxed NSK system. Let $\alpha > 0$ be a given number which we will refer to as the *Korteweg parameter*. We consider for $\varepsilon > 0$ in Ω_T the system

$$\begin{aligned} \rho_t^{\varepsilon,\alpha} + \operatorname{div}(\rho^{\varepsilon,\alpha}\mathbf{v}^{\varepsilon,\alpha}) &= 0, \\ (\rho^{\varepsilon,\alpha}\mathbf{v}^{\varepsilon,\alpha})_t + \operatorname{div}(\rho^{\varepsilon,\alpha}\mathbf{v}^{\varepsilon,\alpha}\otimes\mathbf{v}^{\varepsilon,\alpha} + p(\rho^{\varepsilon,\alpha})\mathbf{I}) &= \operatorname{div}(\mathbf{T}^\varepsilon[v^{\varepsilon,\alpha}]) + \alpha\rho^{\varepsilon,\alpha}\nabla(c^{\varepsilon,\alpha} - \rho^{\varepsilon,\alpha}), \\ -\varepsilon^2\gamma\Delta c^{\varepsilon,\alpha} &= \alpha(\rho^{\varepsilon,\alpha} - c^{\varepsilon,\alpha}). \end{aligned} \tag{16}$$

The system (16) extends the classical NSK system by an additional screened Poisson equation for the new unknown $c^{\varepsilon,\alpha} = c^{\varepsilon,\alpha}(\mathbf{x}, t) \in \mathbb{R}$. Before we discuss the relation between the relaxed NSK system and the NSK system (10) let us present the following result on thermodynamical consistency for (16).

Proposition 2.3. For $\rho_0 : \Omega \to (0, b)$ and $\mathbf{v}_0 : \Omega \to \mathbb{R}^d$ let $(\rho^{\varepsilon,\alpha}, \mathbf{v}^{\varepsilon,\alpha}, c^{\varepsilon,\alpha})$ be a classical solution of (16) which satisfies the initial conditions

$$\rho^{\varepsilon,\alpha}(\cdot, 0) = \rho_0, \ \mathbf{v}^{\varepsilon,\alpha}(\cdot, 0) = \mathbf{v}_0 \text{ in } \Omega \tag{17}$$

and the boundary conditions

$$\mathbf{v}^{\varepsilon,\alpha} = 0,\ \nabla c^{\varepsilon,\alpha} \cdot \mathbf{n} = 0 \text{ in } \partial\Omega. \tag{18}$$

Then we have for $t \in [0, T)$

$$\begin{aligned}\mathcal{E}^{\varepsilon,\alpha}[\rho^{\varepsilon,\alpha}(\cdot,t), \mathbf{v}^{\varepsilon,\alpha}(\cdot,t)c^{\varepsilon,\alpha}(\cdot,\alpha)] - \mathcal{E}^{\varepsilon,\alpha}[\rho_0, \mathbf{v}_0] \\ = -\varepsilon \int_0^t \int_\Omega 2\mu \mathbf{D}(\mathbf{v}^{\varepsilon,\alpha}(\mathbf{x},s)) : \mathbf{D}(\mathbf{v}^{\varepsilon,\alpha}(\mathbf{x},s)) + \lambda(\operatorname{div}(\mathbf{v}^{\varepsilon,\alpha}(\mathbf{x},s)))^2 \, d\mathbf{x}ds.\end{aligned} \tag{19}$$

In (14) we used the relaxed energy

$$\mathcal{E}^{\varepsilon,\alpha}[\rho, \mathbf{v}, c] = \int_\Omega \left(\frac{1}{2}\rho(\mathbf{x})|\mathbf{v}(\mathbf{x})|^2 + W(\rho(\mathbf{x})) + \frac{\alpha}{2}(\rho(\mathbf{x}) - c(\mathbf{x}))^2 + \gamma\varepsilon^2 \frac{|\nabla c(\mathbf{x})|^2}{2} \right) d\mathbf{x}. \tag{20}$$

Proof

We set $d = 2$ and skip the indices ε, α for the proof. Multiply the first three equations in (16) with $-\frac{1}{2}|\mathbf{v}|^2 + W'(\rho)$, v_1, v_2, respectively, add up and integrate with respect to Ω. Using the first boundary condition in (18) it is standard to derive

$$\begin{aligned}\frac{d}{dt}\int_\Omega \frac{1}{2}\rho(\mathbf{x},t)|\mathbf{v}(\mathbf{x},t)|^2 + W(\rho(\mathbf{x},t))\, d\mathbf{x} \\ + \varepsilon \int_\Omega 2\mu \mathbf{D}(\mathbf{v}(\mathbf{x},t)) : \mathbf{D}(\mathbf{v}(\mathbf{x},t)) + \lambda(\operatorname{div}(\mathbf{v}(\mathbf{x},t)))^2 \, d\mathbf{x} \\ = \alpha \int_\Omega \rho(\mathbf{x},t)\mathbf{v}(\mathbf{x},t) \cdot \nabla(c(\mathbf{x},t) - \rho(\mathbf{x},t))\, d\mathbf{x}. \\ = -\alpha \int_\Omega \operatorname{div}(\rho(\mathbf{x},t)\mathbf{v}(\mathbf{x},t))(c(\mathbf{x},t) - \rho(\mathbf{x},t))\, d\mathbf{x} \\ = \alpha \int_\Omega \rho_t(\mathbf{x},t)(c(\mathbf{x},t) - \rho(\mathbf{x},t))\, d\mathbf{x}.\end{aligned} \tag{21}$$

For the last line we used the continuity equation. The elliptic equation in (16) and the second condition in (18) yield

$$\begin{aligned}0 &= \int_\Omega \gamma\varepsilon^2 c_t(\mathbf{x},t)\Delta c(\mathbf{x},t) + \alpha c_t(\mathbf{x},t)(\rho(\mathbf{x},t) - c(\mathbf{x},t))\, d\mathbf{x} \\ &= -\gamma\varepsilon^2 \frac{d}{dt}\int_\Omega \frac{1}{2}|\nabla c|^2(\mathbf{x},t)\, d\mathbf{x} + \int_\Omega \alpha c_t(\mathbf{x},t)(\rho(\mathbf{x},t) - c(\mathbf{x},t))\, d\mathbf{x}.\end{aligned}$$

Thus we obtain with (21) the inequality (19). □

The system (16) can be seen as an approximation of the classical NSK system. For $\varepsilon > 0$ fixed it is expected that solutions $(\rho^{\varepsilon,\alpha}, \mathbf{v}^{\varepsilon,\alpha}, c^{\varepsilon,\alpha})$ of an initial boundary value problem for (16) satisfy $(\rho^{\varepsilon,\alpha},\ c^{\varepsilon,\alpha}) \to (\rho^\varepsilon, \rho^\varepsilon)$ and $\mathbf{v}^{\varepsilon,\alpha} \to \mathbf{v}^\varepsilon$ for the *Korteweg limit* $\alpha \to \infty$ where $(\rho^\varepsilon, \mathbf{v}^\varepsilon)$ is the solution of the corresponding initial boundary value problem for (10). We refer to [8, 9, 14, 19, 20, 21] for first rigorous results on the Korteweg limit. We underline the hypothesis by a numerical example (see Section 3 for the used discretization method).

Example 2.4 (Numerical Verification of the Korteweg Limit)**.** We compute for $d = 1$, $\Omega = (-1, 2)$, and $\varepsilon = 0.01$ a numerical approximation of (16), (17), (18) denoted by $\mathbf{u}_h^{\varepsilon,\alpha} =$

$(\rho_h^{\varepsilon,\alpha}, \rho_h^{\varepsilon,\alpha} v_h^{\varepsilon,\alpha}, c_h^{\varepsilon,\alpha})^T$, and a numerical approximation of (10), (12), (13) denoted by $\mathbf{u}_h^\varepsilon = (\rho^\varepsilon, \rho^\varepsilon v_h^\varepsilon)^T$. The initial datum is

$$\begin{aligned} \rho_0(x) &= \begin{cases} 0.3: & x \in (0.3, 0.6) \cup (0.85, 1.05) \\ 1.8: & \text{else} \end{cases}, \\ v_0(x) &= 0, \end{aligned} \tag{22}$$

which corresponds with (4), (5) to a two-phase density distribution. From the physical point of view, these initial conditions describe two vapour bubbles surrounded by liquid fluid.

In Figure 2 we show the evolution of the density at different times. We observe that the small bubble vanishes and contributes to the bigger bubble at equilibrium. For increasing values of α Table I displays the convergence of the $L^2(\Omega)$-distance of $\mathbf{u}_h^{\varepsilon,\alpha}$ and $\mathbf{u}_h^\varepsilon$ at $t = 5$.

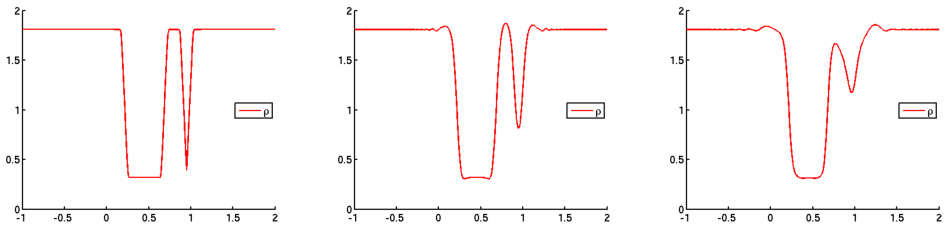

(a) t=0 s (b) t=0.02 s (c) t=0.04 s

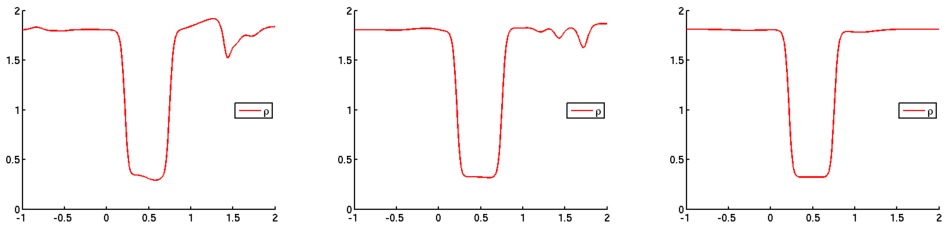

(d) t=0.4 s (e) t=1 s (f) t=4 s

Figure 2. Density evolution for the relaxed NSK system (16) and $\alpha = 100$ with initial datum (22).

i	1	2	3	4	5
α_i	1	5	10	100	1000
$\mathrm{D}_h^i = \|\mathbf{u}_h^{\varepsilon,\alpha_i} - \mathbf{u}_h^\varepsilon\|_{L^2(\Omega)}$, $h = 0.005$	1.039e-1	3.329e-2	1.76e-2	1.526e-3	3.969e-4
$\mathrm{EOC}_i = \frac{\ln(D_h^i/D_h^{i+1})}{\ln(\alpha_{i+1}/\alpha_i)}$	-	0.714	0.902	1.063	0.585
$\mathrm{D}_h^i = \|\mathbf{u}_h^{\varepsilon,\alpha_i} - \mathbf{u}_h^\varepsilon\|_{L^2(\Omega)}$, $h = 0.00125$	1.039e-1	3.333e-2	1.802e-2	1.909e-3	1.683e-4
$\mathrm{EOC}_i = \frac{\ln(D_h^i/D_h^{i+1})}{\ln(\alpha_{i+1}/\alpha_i)}$	-	0.708	0.885	0.975	1.055

Table I. Discrete $L^2(\Omega)$-distance. The distance is decreasing for increasing values of α, indicating the convergence hypothesis.

The numerical results suggest that the relaxed model is an $\mathcal{O}(\alpha^{-1})$-approximation of the original NSK system. Note that the poor EOC $= 0.585$ for $\alpha = 1000$, $h = 0.005$ is due to the fact that the discretization error starts to dominate. □

In fact we will even show that the numerical solution of (16) can be achieved in a more efficient way than that of the original NSK system. In view of Example 2.4 it is then reasonable to compute solutions of the NSK system via solving the approximation (16), cf. Section 4.3 below.
The structural advantage of (16) becomes more evident when we introduce the modified pressure function

$$p_\alpha(\rho) := p(\rho) + \alpha\rho^2/2. \tag{23}$$

We neglect the viscous part of the stress tensor and consider for the sake of simplicity the twodimensional situation. Then the hydrodynamical part of (16) takes the form

$$\begin{pmatrix} \rho^{\varepsilon,\alpha} \\ \rho^{\varepsilon,\alpha} v_1^{\varepsilon,\alpha} \\ \rho^{\varepsilon,\alpha} v_2^{\varepsilon,\alpha} \end{pmatrix}_t + \mathbf{f}_\alpha^1 \left(\begin{pmatrix} \rho^{\varepsilon,\alpha} \\ \rho^{\varepsilon,\alpha} v_1^{\varepsilon,\alpha} \\ \rho^{\varepsilon,\alpha} v_2^{\varepsilon,\alpha} \end{pmatrix} \right)_{x_1} + \mathbf{f}_\alpha^2 \left(\begin{pmatrix} \rho^{\varepsilon,\alpha} \\ \rho^{\varepsilon,\alpha} v_1^{\varepsilon,\alpha} \\ \rho^{\varepsilon,\alpha} v_2^{\varepsilon,\alpha} \end{pmatrix} \right)_{x_2} = \begin{pmatrix} 0 \\ \alpha\rho^{\varepsilon,\alpha} c_{x_1}^{\varepsilon,\alpha} \\ \alpha\rho^{\varepsilon,\alpha} c_{x_2}^{\varepsilon,\alpha} \end{pmatrix} \tag{24}$$

with state vector $\mathbf{u} = (\rho, \rho v_1, \rho v_2)^T$ and $\mathbf{f}_\alpha^{1/2} = \mathbf{f}_\alpha^{1/2}(\mathbf{u})$ defined by

$$\mathbf{f}_\alpha^1(\mathbf{u}) = \left(\rho v_1, \rho v_1^2 + p_\alpha(\rho), \rho v_1 v_2\right)^T, \qquad \mathbf{f}_\alpha^2(\mathbf{u}) = \left(\rho v_2, \rho v_1 v_2, \rho v_2^2 + p_\alpha(\rho)\right)^T.$$

The eigenvalues of the Jacobian $n_1 D\mathbf{f}_\alpha^1(\mathbf{u}) + n_2 D\mathbf{f}_\alpha^2(\mathbf{u}) \in \mathbb{R}^{3\times 3}$ for some vector $\mathbf{n} = (n_1, n_2)^T \in \mathcal{S}^1$ are then

$$\lambda_{\alpha,1}(\mathbf{u}) = \mathbf{v}\cdot\mathbf{n} - \sqrt{p'_\alpha(\rho)}, \qquad \lambda_{\alpha,2}(\mathbf{u}) = \mathbf{v}\cdot\mathbf{n}, \qquad \lambda_{\alpha,3}(\mathbf{u}) = \mathbf{v}\cdot\mathbf{n} + \sqrt{p'_\alpha(\rho)} \tag{25}$$

with corresponding eigenvectors

$$\mathbf{K}_{\alpha,1}(\mathbf{u}) = \begin{pmatrix} 1 \\ v_1 - n_1\sqrt{p'_\alpha(\rho)} \\ v_2 - n_2\sqrt{p'_\alpha(\rho)} \end{pmatrix}, \quad \mathbf{K}_{\alpha,2}(\mathbf{u}) = \begin{pmatrix} 0 \\ n_2 \\ -n_1 \end{pmatrix}, \quad \mathbf{K}_{\alpha,3}(\mathbf{u}) = \begin{pmatrix} 1 \\ v_1 + n_1\sqrt{p'_\alpha(\rho)} \\ v_2 + n_2\sqrt{p'_\alpha(\rho)} \end{pmatrix}. \tag{26}$$

A straightforward computation based on (2) shows that p_α is monotone increasing provided that

$$\alpha > \alpha_* := \frac{|\min\{W''(s) \,:\, s \in (r_1, r_2)\}|}{2}. \tag{27}$$

Then the operator on the right hand side of (24) is hyperbolic in the convex state space

$$\mathcal{U}_\alpha = (0, b) \times \mathbb{R}^2. \tag{28}$$

This property allows us to use shock-capturing schemes that rely on the hyperbolicity of the system (see e.g. [30]). Moreover this structure permits to construct a scheme that obeys the thermodynamical consistency as expressed in Proposition 2.3.

3. LOCAL DISCONTINUOUS GALERKIN SCHEMES FOR NSK SYSTEMS

In this section we provide a Local Discontinuous Galerkin (LDG) scheme, first for the relaxed NSK system, and then for the original NSK system. The most important difference is the discretization of the advective fluxes which in the first case can be done using an approximate Riemann solver while for the second case basically a simple central discretization is reasonable. Note that we skip in this section the indices α and ε on the primal variables.

3.1. A High-Order LDG Approach for the Relaxed NSK System

The idea of the LDG method is to rewrite a given high-order system of equations into a first-order system and discretize it by the DG method [3, 11, 16]. First we introduce some basic notation that is used in the following section. For $d = 1, 2, 3$ let $\mathcal{T}_h = \{\Delta_j | j = 1, \dots, N\}$ be a partition of Ω, where an element Δ_j is an open d-dimensional simplex.We define

$$h_j = \operatorname{diam}(\Delta_j), \qquad h_{j,j'} = \max\{h_j, h_{j'}\}, \qquad h = \sup(h_j) \qquad (j, j' = 1, \dots, N).$$

Denote by $\mathcal{V}_h^m$ the space of elementwise defined polynomials of degree m:

$$\mathcal{V}_h^m = \left\{\phi_h \ : \ \phi_h|_{\Delta_j} \in \mathbb{P}^m(\Delta_j),\ \forall j = 1, \dots, N\right\},$$

where $\mathbb{P}^m(\Delta_j)$ is the space of polynomials of degree m on the simplex Δ_j.

In all numerical experiments we choose quadratic elements for the spatial discretization, and an explicit 3-stage Runge-Kutta scheme for the time discretization [35].
Let some function $\phi_h \in \mathcal{V}_h^m$ be given. With the notations above we define the jump function $[\![\phi_h]\!] = [\![\phi_h^{j,j'}]\!] : \bar{\Delta}_j \cap \bar{\Delta}_{j'} \to \mathbb{R}$ and the average function $\{\phi_h\} = \{\phi_h^{j,j'}\} : \bar{\Delta}_j \cap \bar{\Delta}_{j'} \to \mathbb{R}$ for two elements $\Delta_j, \Delta_{j'}$ $(j, j' \in \{1, \dots, N\})$, which share a $(d-1)$-dimensional cell boundary, by

$$\begin{aligned}
[\![\phi_h^{j,j'}]\!](\boldsymbol{\xi}) &= \lim_{\substack{\mathbf{x}\to\boldsymbol{\xi},\\ (\mathbf{x}-\boldsymbol{\xi})\cdot\mathbf{n}^{j,j'}>0}} \phi_h(\mathbf{x}) - \lim_{\substack{\mathbf{x}\to\boldsymbol{\xi},\\ (\mathbf{x}-\boldsymbol{\xi})\cdot\mathbf{n}^{j',j}>0}} \phi_h(\mathbf{x}) \\
\{\phi_h^{j,j'}\}(\boldsymbol{\xi}) &= \frac{1}{2}\left(\lim_{\substack{\mathbf{x}\to\boldsymbol{\xi},\\ (\mathbf{x}-\boldsymbol{\xi})\cdot\mathbf{n}^{j,j'}>0}} \phi(\mathbf{x}) + \lim_{\substack{\mathbf{x}\to\boldsymbol{\xi},\\ (\mathbf{x}-\boldsymbol{\xi})\cdot\mathbf{n}^{j',j}>0}} \phi_h(\mathbf{x}) \right), \qquad (\boldsymbol{\xi} \in \bar{\Delta}_j \cap \bar{\Delta}_{j'}).
\end{aligned}$$

Thereby $\mathbf{n} = \mathbf{n}^{j,j'} = (n_1^{j,j'}, \dots, n_d^{j,j'}) \in \mathcal{S}^{d-1}$ denotes the constant outer normal of the $(d-1)$-simplex $\bar{\Delta}_j \cap \bar{\Delta}_{j'}$ with respect to Δ_j. Note that the upper indices j, j' are skipped in the sequel when it is clear from the context what element pairing $\Delta_j, \Delta_{j'}$ is meant.

3.1.1. An Approximate Riemann Solver. Before we proceed with the complete description of the LDG method, we introduce a numerical flux derived from an approximate solver for a planar Riemann problem. Let us choose as in (24) $d = 2$ for simplicity and assume $\alpha > \alpha_*$ (see (27)). Consider for $i = 1, 2$ the Riemann problem

$$\mathbf{u}_t + \mathbf{f}_\alpha^i(\mathbf{u})_x = 0, \quad \mathbf{u}(x, 0) = \begin{cases} \mathbf{u}^- \text{ if } x < 0, \\ \mathbf{u}^+ \text{ if } x > 0, \end{cases} \qquad \mathbf{u}^\pm \in \mathcal{U}_\alpha. \tag{29}$$

We recall that by definition of p_α the system in (29) is hyperbolic in the convex state $\mathcal{U}_\alpha$ from (28).

Let us assume to have the case $i = 1$. The most prominent approximate Riemann solver may be the Roe solver from [32]. Roe's approach relies on a linear approximation of (29) such that the Riemann problem is solved exactly for a linear system with flux $\tilde{\mathbf{A}}^1 = \tilde{\mathbf{A}}^1(\mathbf{u}^-, \mathbf{u}^+)\mathbf{u}$ where $\tilde{\mathbf{A}}^1$ is the so-called Roe-matrix with real eigenvalues $\tilde{\lambda}_{\alpha,k}^1$ and eigenvectors $\tilde{\mathbf{K}}_{\alpha,k}^1$, $k = 1, 2, 3$. Together

with some averaged wavestrengths $\tilde{\delta}^1_{\alpha,k} > 0$, the finally needed numerical flux is

$$\tilde{\mathbf{F}}^1_\alpha(\mathbf{u}^-,\mathbf{u}^+) = \ \tfrac{1}{2}(\mathbf{f}^1_\alpha(\mathbf{u}^-)+\mathbf{f}^1_\alpha(\mathbf{u}^+)) - \tfrac{1}{2}\sum_{k=1}^{3}\tilde{\delta}^1_{\alpha,k}|\tilde{\lambda}^1_{\alpha,k}|\tilde{\mathbf{K}}^1_{\alpha,k}. \tag{30}$$

However, Roe matrices are not available for arbitrary pressures as e.g. p_α. Therefore we follow the idea of [23] which provides still a numerical flux $\tilde{\mathbf{F}}^1_\alpha$ as long as the pressure is monotone. We need the quantities

$$\tilde{\rho} = \sqrt{\rho^-\rho^+}, \qquad \tilde{\mathbf{v}} = \frac{\sqrt{\rho^-}\mathbf{v}^- + \sqrt{\rho^+}\mathbf{v}^+}{\sqrt{\rho^-}+\sqrt{\rho^+}}, \qquad \tilde{p}' = \begin{cases} p'_\alpha(\tilde{\rho}) & : \ \rho^- = \rho^+ \\ \frac{p_\alpha(\rho^+)-p_\alpha(\rho^-)}{\rho^+-\rho^-} & : \ \rho^- \neq \rho^+ \end{cases}.$$

Since $\alpha > \alpha_*$ the following generalized averaged wavestrengths, eigenvalues and eigenvectors $\tilde{\delta}^1_{\alpha,k}$, $\tilde{\lambda}^1_{\alpha,k}$, $\tilde{\mathbf{K}}^1_{\alpha,k}$ are well-defined.

$$\begin{aligned}
&\tilde{\delta}^1_{\alpha,1} = \frac{1}{2}\left[[\![\rho]\!] - \tilde{\rho}\frac{[\![v_1]\!]}{\sqrt{\tilde{p}'}}\right], && \tilde{\delta}^1_{\alpha,2} = \tilde{\rho}[\![v_2]\!], && \tilde{\delta}^1_{\alpha,3} = \frac{1}{2}\left[[\![\rho]\!] + \tilde{\rho}\frac{[\![v_1]\!]}{\sqrt{\tilde{p}'}}\right],\\
&\tilde{\lambda}^1_{\alpha,1} = \tilde{v}_1 - \sqrt{\tilde{p}'}, && \tilde{\lambda}^1_{\alpha,2} = \tilde{v}_1, && \tilde{\lambda}^1_{\alpha,3} = \tilde{v}_1 + \sqrt{\tilde{p}'},\\
&\tilde{\mathbf{K}}^1_{\alpha,1} = \begin{pmatrix} 1 \\ \tilde{v}_1 - \sqrt{\tilde{p}'} \\ \tilde{v}_2 \end{pmatrix}, && \tilde{\mathbf{K}}^1_{\alpha,2} = \begin{pmatrix} 0 \\ 0 \\ 1 \end{pmatrix}, && \tilde{\mathbf{K}}^1_{\alpha,3} = \begin{pmatrix} 1 \\ \tilde{v}_1 + \sqrt{\tilde{p}'} \\ \tilde{v}_2 \end{pmatrix}.
\end{aligned}$$

We used $[\![s]\!] = s^+ - s^-$ for some s. With these values we obtain then a numerical flux $\tilde{\mathbf{F}}^1_\alpha$ by (30). The flux $\tilde{\mathbf{F}}^2_\alpha$ is derived in the analogous way.

Remark 3.1. The construction of the flux relies heavily on the hyperbolicity of (29) in $\mathcal{U}_\alpha$. It can only be used for a monotonically increasing pressure function p_α. Instead of a Roe-like flux, any other hyperbolic solver that can deal with the pressure law provided by p_α can be used. We choose this one because it turned out to be very robust in our numerical experiments.

3.1.2. Complete LDG Scheme for the Relaxed NSK System. In this section we present the discretization for the twodimensional relaxed NSK system (16). We start with the equations for density and momentum, and assume for the moment that the additional unknown $c : \Omega_T \to \mathbb{R}$ is given. The system (16) is rewritten as the first-order system

$$\begin{pmatrix} q \\ r \end{pmatrix} - \boldsymbol{\mathcal{L}}^1[\mathbf{w}] = 0, \qquad \begin{pmatrix} \rho \\ m_1 \\ m_2 \end{pmatrix}_t + \boldsymbol{\mathcal{L}}^2[\mathbf{w}] = 0 \tag{31}$$

for the unknown $\mathbf{w} := (\mathbf{u}, q, r) : \Omega_T \to \mathcal{U}_\alpha \times \mathbb{R}^2$. The first-order differential operators $\boldsymbol{\mathcal{L}}^1$, $\boldsymbol{\mathcal{L}}^2$ are defined by

$$\begin{aligned}
\boldsymbol{\mathcal{L}}^1[\mathbf{w}] &= \begin{pmatrix} v_1 \\ -v_2 \end{pmatrix}_{x_1} + \begin{pmatrix} v_2 \\ v_1 \end{pmatrix}_{x_2},\\
\boldsymbol{\mathcal{L}}^2[\mathbf{w}] &= \left(\mathbf{f}^1_\alpha(\mathbf{u}) + \begin{pmatrix} 0 \\ -\varepsilon\lambda q \\ \varepsilon\mu r \end{pmatrix}\right)_{x_1} + \left(\mathbf{f}^2_\alpha(\mathbf{u}) + \begin{pmatrix} 0 \\ -\varepsilon\mu r \\ -\varepsilon\lambda q \end{pmatrix}\right)_{x_2} + \begin{pmatrix} 0 \\ -\alpha\rho c_{x_1} \\ -\alpha\rho c_{x_2} \end{pmatrix}.
\end{aligned} \tag{32}$$

To discretize (31) consider elements $\Delta_j, \Delta_{j'}$ with joint edge and associated outer normal $\mathbf{n} = \mathbf{n}^{j,j'} \in \mathcal{S}^1$. Define for discrete functions $\mathbf{w}_h, c_h$ and $\boldsymbol{\xi} \in \bar{\Delta}_j \cap \bar{\Delta}_{j'}$ the discrete flux-like terms

$$\begin{aligned}
\mathbf{g}^1_{j,j'}(\boldsymbol{\xi}; \mathbf{w}_h) &= \begin{pmatrix} \{v_{1,h}\}n_1 + \{v_{2,h}\}n_2 \\ \{-v_{2,h}\}n_1 + \{v_{1,h}\}n_2 \end{pmatrix}, \qquad \mathbf{v}_h = \frac{\mathbf{m}_h}{\rho_h}, \\
\mathbf{g}^2_{j,j'}(\boldsymbol{\xi}; \mathbf{w}_h) &= \tilde{\mathbf{F}}^1_\alpha(\mathbf{w}_h|_{\Delta_j}(\boldsymbol{\xi}), \mathbf{w}_h|_{\Delta_{j'}}(\boldsymbol{\xi}))n_1 + \tilde{\mathbf{F}}^2_\alpha(\mathbf{w}_h|_{\Delta_j}(\boldsymbol{\xi}), \mathbf{w}_h|_{\Delta_{j'}}(\boldsymbol{\xi}))n_2 \\
&\quad + \begin{pmatrix} 0 \\ -\varepsilon\lambda\{q_h\}n_1 - \varepsilon\mu\{r_h\}n_2 + \alpha\{\rho_h\}[\![c_h]\!] \\ \varepsilon\mu\{r_h\}n_1 - \varepsilon\lambda\{q_h\}n_2 + \alpha\{\rho_h\}[\![c_h]\!] \end{pmatrix}.
\end{aligned} \tag{33}$$

The functions $\tilde{\mathbf{F}}^{1/2}_\alpha$ in (33) are the numerical fluxes that were introduced in Section 3.1.1. The third term in $(32)_2$ is a non-conservative flux term that requires an extra treatment. We adopt the discretization for the nonconservative term from [16, 15]. Note that we have suppressed in (33) the dependence of the jump/average functions on $\boldsymbol{\xi}$.

To account for the boundary conditions (18) we introduce for each edge of an element Δ_j which is part of $\partial\Omega$ an associated ghost element, call it $\Delta_{j'}$. A discrete function $\mathbf{w}_h$ is naturally extended to these elements by setting

$$\begin{aligned}
&\rho_h|_{\Delta_{j'}} = \rho_h|_{\Delta_j}, \quad \mathbf{v}_h|_{\Delta_{j'}} \cdot \mathbf{n}^{j,j'} = -\mathbf{v}_h|_{\Delta_j} \cdot \mathbf{n}^{j,j'}, \quad \mathbf{v}_h|_{\Delta_{j'}} \cdot \mathbf{t}^{j,j'} = \mathbf{v}_h|_{\Delta_j} \cdot \mathbf{t}^{j,j'}, \\
&q_h|_{\Delta_{j'}} = q_h|_{\Delta_j}, \quad r_h|_{\Delta_{j'}} = r_h|_{\Delta_j}, \qquad\qquad\qquad c_h|_{\Delta_{j'}} = c_h|_{\Delta_j},
\end{aligned} \tag{34}$$

and the numerical boundary flux $\mathbf{g}^1_{j,j'}$ is defined as in (33) but

$$\begin{aligned}
\mathbf{g}^2_{j,j'}(\boldsymbol{\xi}; \mathbf{w}_h) &= \tilde{\mathbf{F}}^1_\alpha(\mathbf{w}_h|_{\Delta_j}(\boldsymbol{\xi}), \mathbf{w}_h|_{\Delta_{j'}}(\boldsymbol{\xi}))n_1 + \tilde{\mathbf{F}}^2_\alpha(\mathbf{w}_h|_{\Delta_j}(\boldsymbol{\xi}), \mathbf{w}_h|_{\Delta_{j'}}(\boldsymbol{\xi}))n_2 \\
&\quad + \begin{pmatrix} 0 \\ -\varepsilon\lambda\{q_h\}n_1 - \varepsilon\mu\{r_h\}n_2 \\ \varepsilon\mu\{r_h\}n_1 - \varepsilon\lambda\{q_h\}n_2 \end{pmatrix}.
\end{aligned} \tag{35}$$

Now we can present the scheme for the hydromechanical part (24). Let $c_h : [0,T] \to \mathcal{V}^m_h$ be given and denote by $\mathcal{E}(j)$ the set of all indices of the (ghost) elements which share a joint edge with $\Delta_{j'}$. We search for a function $\mathbf{w}_h = \mathbf{w}_h(t) : [0,T] \to (\mathcal{V}^m_h)^5$ that satisfies for $j = 1, \dots, N$, $t \in (0,T)$, and all $\phi_h \in \mathcal{V}^m_h$ with $\phi_h|_{\partial\Omega} = 0$ the differential equations

$$\begin{aligned}
&\sum_{j=1}^N \int_{\Delta_j} \left(\begin{pmatrix} q_h \\ r_h \end{pmatrix} \phi_h + \begin{pmatrix} v_{1,h} \\ -v_{2,h} \end{pmatrix} \phi_{h,x_1} + \begin{pmatrix} v_{2,h} \\ v_{1,h} \end{pmatrix} \phi_{h,x_2} \right) d\mathbf{x} \\
&\qquad = \sum_{j=1}^N \sum_{j \in \mathcal{E}(j)} \int_{\bar{\Delta}_j \cap \bar{\Delta}_{j'}} \mathbf{g}^1_{j,j'}(\boldsymbol{\xi}, \mathbf{w}_h)[\![\phi_h{}^{j,j'}]\!](\boldsymbol{\xi})\, d\boldsymbol{\xi},
\end{aligned}$$

$$\begin{aligned}
&\sum_{j=1}^N \int_{\Delta_j} \left[\mathbf{u}_{h,t}\phi_h - \left(\mathbf{f}^1_\alpha(\mathbf{u}_h) + \begin{pmatrix} 0 \\ -\varepsilon\lambda q_h \\ \varepsilon\mu r_h \end{pmatrix} \right) \phi_{h,x_1} - \left(\mathbf{f}^1_\alpha(\mathbf{u}_h) + \begin{pmatrix} 0 \\ -\varepsilon\lambda r_h \\ -\varepsilon\lambda q_h \end{pmatrix} \right) \phi_{h,x_2} \right. \\
&\qquad \left. - \begin{pmatrix} 0 \\ \alpha\rho_h c_{h,x_1} \\ \alpha\rho_h c_{h,x_2} \end{pmatrix} \phi_h \right] d\mathbf{x} + \sum_{j=1}^N \sum_{j' \in \mathcal{E}(j)} \int_{\bar{\Delta}_j \cap \bar{\Delta}_{j'}} \mathbf{g}^2_{j,j'}(\boldsymbol{\xi}; \mathbf{w}_h)[\![\phi_h^{j,j'}]\!](\boldsymbol{\xi})\, d\boldsymbol{\xi} = 0,
\end{aligned} \tag{36}$$

$$\rho_h(.,0) = \mathcal{P}_h\rho_0, \qquad\qquad \mathbf{v}_h(.,0) = \mathcal{P}_h\mathbf{v}_0.$$

Here $\mathcal{P}_h$ denoted the L^2-projection to the space $\mathcal{V}_h^m$.

In all numerical experiments we choose quadratic elements for the spatial discretization, and an explicit 3-stage Runge-Kutta scheme for the time discretization [35].

It remains to give the discretization of the elliptic constraint. For that issue we follow [31]. The projection of the exact solution c of the elliptic equation (16) is supposed to fulfill $[\![c]\!] = 0$ for $\partial\Delta_j \notin \partial\Omega$. Since this is not guaranted for discontinuous Galerkin approximate solutions, we introduce for $\sigma^0,\ \sigma^1 > 0,\ \chi \in \mathbb{R}$ and $\phi_h, \psi_h \in \mathcal{V}_h^m$ the penalty terms

$$\begin{aligned} J_0^j(\psi_h,\phi_h) &= \sum_{j'\in\mathcal{E}(j)} \frac{\sigma^0}{h_{j,j'}} \int_{\bar\Delta_j\cap\bar\Delta_{j'}} [\![\psi_h]\!][\![\phi_h]\!]\, d\boldsymbol{\xi}, \\ J_1^j(\psi_h,\phi_h) &= \sum_{j'\in\mathcal{E}(j)} \frac{\sigma^1}{h_{j,j'}} \int_{\bar\Delta_j\cap\bar\Delta_{j'}} [\![\nabla\psi_h]\!]\cdot[\![\nabla\phi_h]\!]\, d\boldsymbol{\xi}, \qquad (j=1,\dots,N). \\ J_\chi^j(\psi_h,\phi_h) &= \chi \sum_{j'\in\mathcal{E}(j)} \int_{\bar\Delta_j\cap\bar\Delta_{j'}} [\![\nabla\phi_h\cdot\mathbf{n}]\!]\{\psi_h\}\, d\boldsymbol{\xi}, \end{aligned} \tag{37}$$

The terms $J_0,\ J_1,\ J_\chi$ penalize the the jump of some function ϕ (or ψ) and the jump of its derivative. These penalty terms guarantee the stability of the numerical scheme and the uniqueness of the discrete solution c_h. We refer to [31] for more details. In this paper we choose $\sigma^0 = \sigma^1 = \chi = 1$.

Let now $\rho_h = \rho_h(\mathbf{x},t)$ with $\rho_h(.,t) \in \mathcal{V}_h^m$ for $t \in [0,T]$ be given. We search for $c_h = c_h(\mathbf{x},t)$ with $c_h(.,t) \in \mathcal{V}_m^h$ such that for all $\phi \in \mathcal{V}_h^m$ with $\nabla\phi_h\cdot\mathbf{n} = 0$ on $\partial\Delta_j\cap\partial\Omega$ and $j = 1,\dots,N$ we have

$$\begin{aligned} \sum_{j=1}^N \left(\int_{\Delta_j} (\gamma\varepsilon^2 \nabla c_h\cdot\nabla\phi_h + \alpha c_h\phi_h)\, d\mathbf{x} - \gamma\varepsilon^2 \sum_{j'\in\mathcal{E}(j)} \int_{\bar\Delta_j\cap\bar\Delta_{j'}} \left(\nabla c_h\cdot\mathbf{n}^{j,j'}\right)\phi_h\, d\boldsymbol{\xi} \right) \\ = \sum_{j=1}^N \left(\int_{\Delta_j} \alpha\rho_h\phi_h\, d\mathbf{x} - J_0^j(c_h,\phi_h) - J_1^j(c_h,\phi_h) - J_\chi^j(c_h,\phi_h) \right. \\ \left. + \int_{\partial\Delta_j\cap\partial\Omega} \frac{\sigma^1}{h_{j,j'}} [\![\nabla c_h]\!][\![\nabla\phi_h]\!] ds \right). \end{aligned} \tag{38}$$

From (36) and (38) we get the complete approximate solution

$$\mathbf{z}_h^{\varepsilon,\alpha} = (\mathbf{u}_h^T, c_h)^T = (\rho_h, \rho_h\mathbf{v}_h^T, c_h)^T.$$

In one space dimension the mass matrix has a block diagonal structure and thus we can use a computationally cheap LU factorization. If the mesh is fixed for all time steps we have to do this factorization only once. This helps us to achieve good performance in solving (38). In higher space dimensions we use adaptive mesh refinement to reduce the computational costs. Thus, we must solve (38) in each time step. We make use of the symmetry of the linear system and use a cg-solver. In our numerical tests, we used a residual error estimator and needed less than ten iterations to achieve a residual tolerance below 10^{-8}.

3.2. A High-Order LDG scheme for the original NSK system

For the sake of completeness and to highlight the structural properties of the original third-order NSK system (10) we provide also its LDG discretization in some detail. It is done in a similar way

as the discretization for the relaxed NSK system (16). We have here with analogous notations the first-order system

$$\begin{pmatrix} k \\ l \\ q \\ r \end{pmatrix} - \boldsymbol{\mathcal{L}}^1[\mathbf{w}] = 0, \qquad s - \boldsymbol{\mathcal{L}}^2[\mathbf{w}] = 0, \qquad \begin{pmatrix} \rho \\ m_1 \\ m_2 \end{pmatrix}_t + \boldsymbol{\mathcal{L}}^3[\mathbf{w}] = 0 \tag{39}$$

for the unknown $\mathbf{w} := (\mathbf{u}, k, l, q, r, s) : \Omega_T \to \mathcal{U}_\alpha \times \mathbb{R}^5$. Of course the parameter α has no meaning in this context but the state space remains the same and we therefore keep this notation. The first-order differential operators $\boldsymbol{\mathcal{L}}^1$, $\boldsymbol{\mathcal{L}}^2$, $\boldsymbol{\mathcal{L}}^3$ are defined by

$$\begin{aligned} \boldsymbol{\mathcal{L}}^1[\mathbf{w}] &= \begin{pmatrix} \rho \\ 0 \\ v_1 \\ -v_2 \end{pmatrix}_{x_1} + \begin{pmatrix} 0 \\ \rho \\ v_2 \\ v_1 \end{pmatrix}_{x_2}, \qquad \boldsymbol{\mathcal{L}}^2[\mathbf{w}] = k_{x_1} + l_{x_2}, \\ \boldsymbol{\mathcal{L}}^3[\mathbf{w}] &= \left(\mathbf{f}^1(\mathbf{u}) + \begin{pmatrix} 0 \\ -\varepsilon\lambda q \\ \varepsilon\mu r \end{pmatrix} \right)_{x_1} + \left(\mathbf{f}^1(\mathbf{u}) + \begin{pmatrix} 0 \\ -\varepsilon\mu r \\ -\varepsilon\lambda q \end{pmatrix} \right)_{x_2} - \begin{pmatrix} 0 \\ \gamma\varepsilon^2 \rho s_{x_1} \\ \gamma\varepsilon^2 \rho s_{x_2} \end{pmatrix}. \end{aligned} \tag{40}$$

Note that the second term in $(40)_2$ is again a non-conservative term. We choose as numerical fluxes for some discrete function $\mathbf{w}_h$ at the inner cell interfaces

$$\mathbf{g}^1_{j,j'}(\boldsymbol{\xi}, \mathbf{w}_h) = \begin{pmatrix} \{\rho_h\} n_1 \\ \{\rho_h\} n_2 \\ \{v_{1,h}\} n_1 + \{v_{2,h}\} n_2 \\ -\{v_{2,h}\} n_1 + \{v_{1,h}\} n_2 \end{pmatrix}, \qquad \mathbf{g}^2_{j,j'}(\boldsymbol{\xi}; \mathbf{w}_h) = \{k\} n_1 + \{l\} n_2,$$

$$\mathbf{g}^3_{j,j'}(\boldsymbol{\xi}; \mathbf{w}_h) = \begin{pmatrix} \{m_{1,h}\} n_1 + \{m_{2,h}\} n_2 \\ \{v^2_{1,h}\rho_h + p(\rho_h) - \varepsilon\lambda q_h\} n_1 + \{v_{1,h} v_{2,h} \rho_h - \varepsilon\mu r_h\} n_2 \\ \{v_{1,h} v_{2,h} \rho_h + \varepsilon\mu r_h\} n_1 + \{v^2_{2,h}\rho_h + p(\rho_h) - \varepsilon\lambda q_h\} n_2 \end{pmatrix} - \begin{pmatrix} 0 \\ \gamma\varepsilon^2 \{\rho_h\} [\![s_h]\!] \\ \gamma\varepsilon^2 \{\rho_h\} [\![s_h]\!] \end{pmatrix}.$$

Because the first-order part of system (10) is of mixed hyperbolic-elliptic type, one can only use central differences as numerical fluxes and not the more sophisticated Riemann solver that was presented in Section 3.1.1. For the nonconservative flux we follow the same path as in (33). In order to obey the boundary conditions (13) we set (using the same set-up as in (34)) for the ghost elements

$$\begin{gathered} \rho_h|_{\Delta_{j'}} = \rho_h|_{\Delta_j}, \mathbf{v}_h|_{\Delta_{j'}} \cdot \mathbf{n}^{j,j'} = -\mathbf{v}_h|_{\Delta_j} \cdot \mathbf{n}^{j,j'}, \mathbf{v}_h|_{\Delta_{j'}} \cdot \mathbf{t}^{j,j'} = \mathbf{v}_h|_{\Delta_j} \cdot \mathbf{t}^{j,j'}, \\ q_h|_{\Delta_{j'}} = q_h|_{\Delta_j}, \quad r_h|_{\Delta_{j'}} = r_h|_{\Delta_j}, \quad s_h|_{\Delta_{j'}} = s_h|_{\Delta_j}, \quad \nabla\rho_h|_{\Delta_{j'}} \cdot \mathbf{n}^{j,j'} = -\nabla\rho_h|_{\Delta_j} \cdot \mathbf{n}^{j,j'}. \end{gathered}$$

With this choice the fluxes at the boundary can be exactly chosen as the inner fluxes $\mathbf{g}^1_{j,j'}$, $\mathbf{g}^2_{j,j'}$, $\mathbf{g}^3_{j,j'}$ above.

With these preparations we obtain the semidiscrete numerical scheme

$$\sum_{j=1}^{N}\int_{\Delta_j}\left(\begin{pmatrix}k_h\\ l_h\\ q_h\\ r_h\end{pmatrix}\phi_h+\begin{pmatrix}\rho_h\\ 0\\ v_{1,h}\\ -v_{2,h}\end{pmatrix}\phi_{h,x_1}+\begin{pmatrix}0\\ \rho_h\\ v_{2,h}\\ v_{1,h}\end{pmatrix}\phi_{h,x_2}\right)d\mathbf{x}$$
$$=\sum_{j=1}^{N}\sum_{j'\in\mathcal{E}(j)}\int_{\bar\Delta_j\cap\bar\Delta_{j'}}\mathbf{g}^1_{j,j'}(\boldsymbol{\xi},\mathbf{w}_h)[\![\phi_h]\!](\boldsymbol{\xi})\,d\boldsymbol{\xi},$$

$$\sum_{j=1}^{N}\int_{\Delta_j}s_h\phi_h\,d\mathbf{x}+\sum_{j=1}^{N}\int_{\Delta_j}k_h\phi_{h,x_1}+l_h\phi_{h,x_2}\,d\mathbf{x}$$
$$=\sum_{j=1}^{N}\sum_{j'\in\mathcal{E}(j)}\int_{\bar\Delta_j\cap\bar\Delta_{j'}}\mathbf{g}^2_{j,j'}(\boldsymbol{\xi},\mathbf{w}_h)[\![\phi_h]\!](\boldsymbol{\xi})\,d\boldsymbol{\xi}, \tag{41}$$

$$\sum_{j=1}^{N}\int_{\Delta_j}\left[\mathbf{u}_{h,t}\phi_h-\left(\mathbf{f}^1(\mathbf{u}_h)+\begin{pmatrix}0\\ -\varepsilon\lambda q_h\\ \varepsilon\mu r_h\end{pmatrix}\right)\phi_{h,x_1}-\left(\mathbf{f}^2(\mathbf{u}_h)+\begin{pmatrix}0\\ -\varepsilon\lambda r_h\\ -\varepsilon\lambda q_h\end{pmatrix}\right)\phi_{h,x_2}\right.$$
$$\left.-\begin{pmatrix}0\\ \alpha\rho_h s_{h,x_1}\\ \alpha\rho_h s_{h,x_2}\end{pmatrix}\phi_h\right]d\mathbf{x}+\sum_{j=1}^{N}\sum_{j'\in\mathcal{E}(j)}\int_{\bar\Delta_j\cap\bar\Delta_{j'}}\mathbf{g}^3_{j,j'}(\boldsymbol{\xi},\mathbf{w}_h)[\![\phi_h]\!](\boldsymbol{\xi})\,d\boldsymbol{\xi}=0,$$

$$\rho_h(.,0)=\mathcal{P}_h\rho_0,\qquad \mathbf{v}_h(.,0)=\mathcal{P}_h\mathbf{v}_0.$$

Altogether we get the approximate solution

$$\mathbf{u}_h^\varepsilon=\mathbf{u}_h=(\rho_h,\mathbf{v}_h^T)^T.$$

4. NUMERICAL EXPERIMENTS WITH LOCAL DISCONTINUOUS GALERKIN SCHEMES

We present a series of results that show the superior performance of the new system in situations relevant for phase transitions. The numerical solutions for the one- and twodimensional NSK systems (10) and (16) are computed with the numerical schemes that we presented in Section 3.1 and the model parameters as in (4). In all computations we set $\Omega=(-1,2)$ for $d=1$ and $\Omega=(0,1)^2$ for $d=2$.

4.1. Sharp-Interface Limit

We consider systems (10) and (16) for $d=1,2$. For $d=1$ we start with initial conditions

$$\rho_0(x)=\begin{cases}0.3, & x\in(0.3,0.6)\\ 1.8, & \text{else}\end{cases}$$
$$v_0(x)=0.$$

and set $h=0.005$, $\gamma=1$, $\alpha=100$. The initial datum is a nonequilibrium bubble that will be driven towards two-phase equilibrium by the evolution of the NSK systems.

We want to investigate how the discretization method for the two systems can deal with tiny

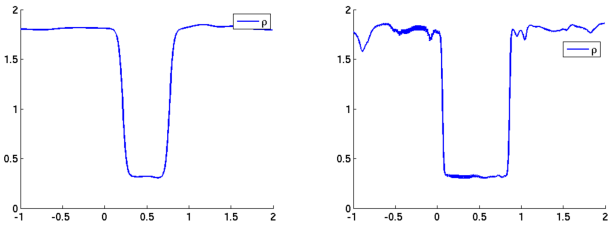

(a) NSK, $\varepsilon = 0.01$ (b) NSK, $\varepsilon = 0.001$

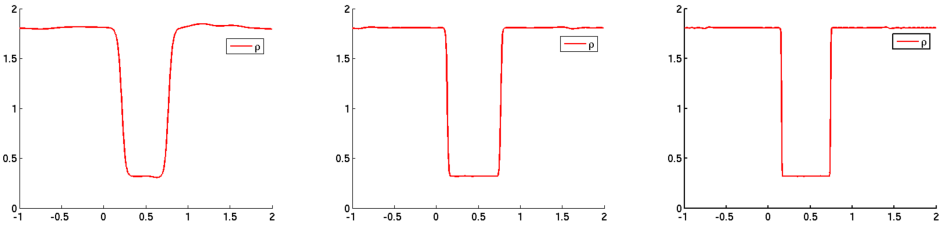

(c) Relaxed NSK, $\varepsilon = 0.01$ (d) Relaxed NSK, $\varepsilon = 0.001$ (e) Relaxed NSK, $\varepsilon = 0.0001$

Figure 3. The first row (second row) displays the approximate solutions at $t = 1.72$ for the original NSK system (10) (the relaxed NSK system (16)) for different values of ε. The interface parameter ε decreases from left to right. The interface gets sharper from left to right for the relaxed NSK system, but the approximate solution remains stable. For $\varepsilon = 0.001$ we observe severe oscillations for the original NSK system. A computation for $\varepsilon = 0.0001$ fails due to the occurence of negative densities.

interfaces which appear in the sharp interface limit ($\varepsilon \to 0$) for fixed h. Figure 3 shows, that the method for system (10) is not able to deal with phase transitions for $\varepsilon < 0.001$, while system (16) has no problems with the SI-Limit. Note that it is possible to obtain a reasonable numerical solution for the NSK system (10) if we choose $h < \varepsilon$. This means that the interface is resolved by the underlying grid. For the relaxed NSK system we obtain numerical solutions even for underresolved interfaces. Even more interesting is the evolution of the energies $\mathcal{E}^\varepsilon$ and $\mathcal{E}^{\varepsilon,\alpha}$ (see Propositions 2.1, 2.3) which are dissipated by the exact solution. The numerical scheme for the relaxed NSK system leads to perfectly monotone decay of the associated energy while the numerical method for the original NSK system does not preserve the energy decay (Figure 4). Let us note that we are not able to prove this property for this scheme, therefore another discretization is presented in Section 5 below.

4.2. Large Density Variations

Another problem of the numerical methods for the NSK system (10) is, that they are not able to deal with large density jumps. As we explained above, the first-order part of the system is of mixed hyperbolic-elliptic type and one can merely use central differences as numerical fluxes. With these fluxes, there is no chance to stabilize the numerical scheme for large density gradients. We can overcome this problem, if we use the relaxed NSK system (16).

We introduce a modified version of the Van-der-Waals pressure equation (3)

$$p^s(\rho) = s \cdot p\left(\frac{\rho}{s}\right),$$

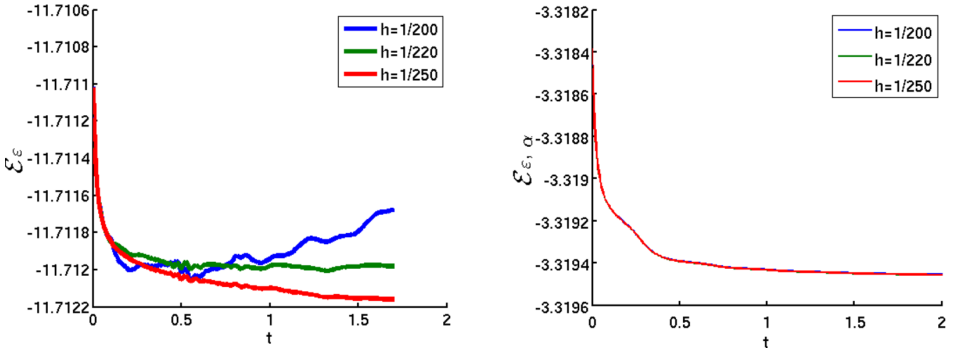

(a) NSK, $\varepsilon = 0.002$ (b) Relaxed NSK, $\varepsilon = 0.0001,\ \alpha = 100$

Figure 4. Evolution of the energy (15) for the NSK system (left) and energy (20) for the relaxed NSK system (right). It can be expected that the oscillations for $\mathcal{E}^\varepsilon$ vanish for $h \to 0$.

with the scaling parameter $s = 200$ to enlarge the elliptic region (cf. (5)). This enables large density jumps for phase boundaries.

We set with $d = 1$ the initial conditions

$$\begin{aligned} \rho_0(x) &= \begin{cases} 150, & x \in \bigcup_{k=0}^{14} (0.08 + 0.05k, 0.12 + 0.05k) \\ 120, & \text{else} \end{cases} \\ v_0(x) &= 0. \end{aligned} \tag{42}$$

and $\alpha = 100, 10000,\ h = 0.001,\ \varepsilon = 0.01,\ \gamma = 1.$

This corresponds to a perturbed fluid state in the elliptic region. The solution is driven to a two-phase equilibrium with a large density variation by a factor of 200. The results for two values of α are displayed in Figure 5, it is possible to simulate large density ratios with the relaxed NSK system whereas the direct discretization for the NSK system is not able to simulate these jumps.

4.3. *Computational Efficiency*

We again consider systems (10) and (16) and use the same initial conditions as in example 2.4. In this test case we use the numerical method for the relaxed NSK model to approximate solutions of the NSK system. Thus we have an error due to the discretization and due to the choice of the Korteweg parameter α. We compute

$$\begin{aligned} \|.\|^\alpha_{L^2} &:= \|u^\varepsilon_{0.00125}(.,t) - u^{\varepsilon,\alpha}_h(.,t)\|_{L^2(\Omega)}, \\ \|.\|_{L^2} &:= \|u^\varepsilon_{0.00125}(.,t) - u^\varepsilon_h(.,t)\|_{L^2(\Omega)} \end{aligned}$$

at $t = 5$ for different values of $h \geq 0.0025$ and α. Here $u^\varepsilon_{0.00125}$ acts as our (quasi-exact) reference solution. We take the results of Table II as numerical evidence, that $u^h_\alpha \to u^h$ for $\alpha \to \infty$. Moreover the results show that it might be an advantage to use system (16) for directly computing solutions for (10).

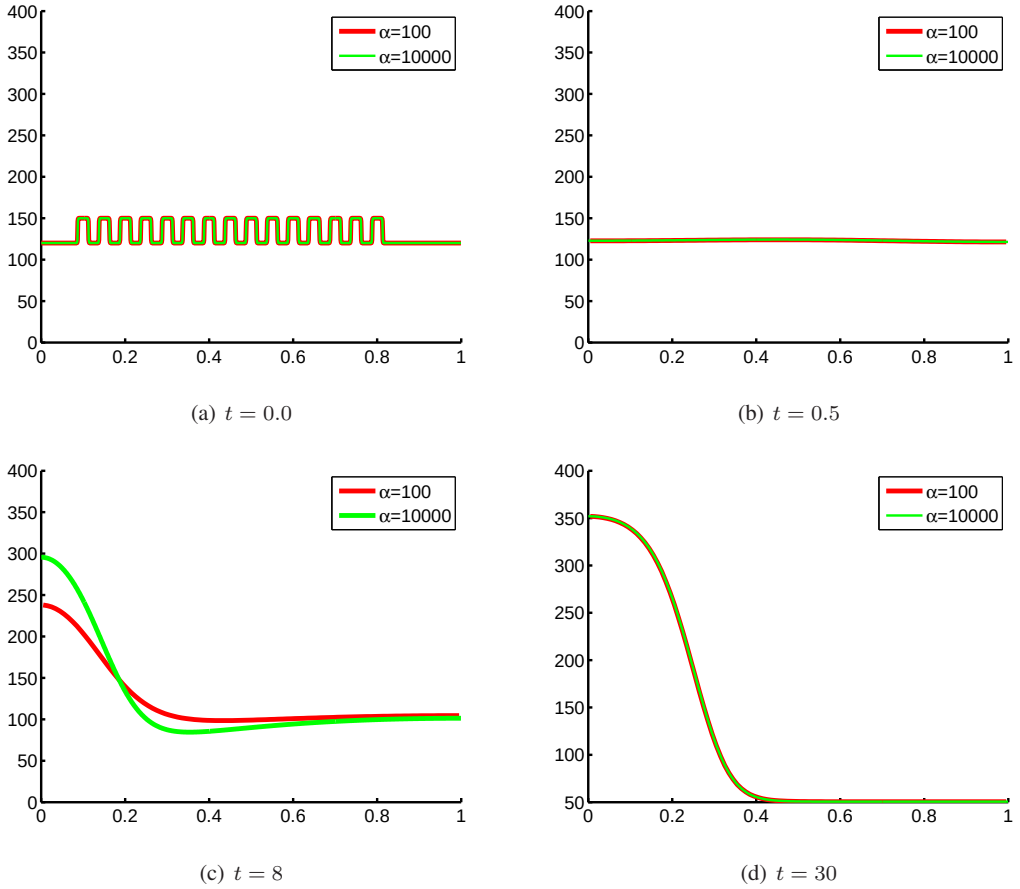

(a) $t = 0.0$ (b) $t = 0.5$

(c) $t = 8$ (d) $t = 30$

Figure 5. Time evolution of the density for a setting which leads to large density variations using the relaxed NSK system

4.4. 2D Testcase: Static Equilibrium

We compute numerical solutions to the relaxed NSK system (16) in 2D. We start with a set of 22 vapour bubbles in a bounded box $\Omega = (0,1)^2$ filled with liquid. Figure (6) shows the density distribution at different times. This test case shows that we can expect, that the relaxed NSK system is also able to describe the behaviour of a two-phase system correctly for $d = 2$.

5. A THERMODYNAMICALLY CONSISTENT DISCRETIZATION

We introduce now a numerical discretization for the relaxed NSK system (16) that satisfies a discrete analogue of the energy dissipation inequality for exact solutions as stated in Proposition 2.3. To this end we consider the onedimensional system on the real line, i.e. $\Omega = \mathbb{R}$

$$\begin{aligned} \begin{pmatrix} \rho^{\varepsilon,\alpha} \\ \rho^{\varepsilon,\alpha} v^{\varepsilon,\alpha} \end{pmatrix}_t + \mathbf{f}_\alpha \begin{pmatrix} \rho^{\varepsilon,\alpha} \\ \rho^{\varepsilon,\alpha} v^{\varepsilon,\alpha} \end{pmatrix}_x &= \begin{pmatrix} 0 \\ \varepsilon\beta v_{xx}^{\varepsilon,\alpha} + \alpha\rho^{\varepsilon,\alpha} c_x^{\varepsilon,\alpha} \end{pmatrix}, \\ -\varepsilon^2\gamma c_{xx}^{\varepsilon,\alpha} &= \alpha(\rho^{\varepsilon,\alpha} - c^{\varepsilon,\alpha}). \end{aligned} \tag{43}$$

α	$\Delta x =$	0.02	0.01	0.005	0.0025
1	CPU-time [s]	28	114	563	3990
	$\|.\|_{L^2}^{\alpha}$	0.365	0.288	0.205	0.14
5	CPU-time [s]	30	104	585	3499
	$\|.\|_{L^2}^{\alpha}$	0.108	0.085	0.061	0.044
10	CPU-time [s]	28	104	754	3459
	$\|.\|_{L^2}^{\alpha}$	0.048	0.044	0.033	0.023
100	CPU-time [s]	35	113	687	3330
	$\|.\|_{L^2}^{\alpha}$	0.013	1.4e-3	2.9e-3	2.4e-3
1000	CPU-time [s]	97	213	828	3347
	$\|.\|_{L^2}^{\alpha}$	0.016	2.4e-3	2.4e-4	1.3e-4
10000	CPU-time [s]	287	870	2178	4795
	$\|.\|_{L^2}^{\alpha}$	0.016	2.1e-3	3.7e-4	7.2e-05
∞	CPU–time [s]	38	123	662	6046
	$\|.\|_{L^2}$	0.038	5.7e-3	6.4e-4	9.7e-05

Table II. Computational times and $\|.\|_{L^2}^{\alpha}$, $\|.\|_{L^2}$. We observe that, for each h, we can compute approximate solutions with model (16) that have the same error $\|.\|_{L^2}^{\alpha}$ as the error $\|.\|_{L^2}$ for the approximate solutions for model (10) with equal or even less computional costs. This is possible because of the more severe time step restrictions for model (10).

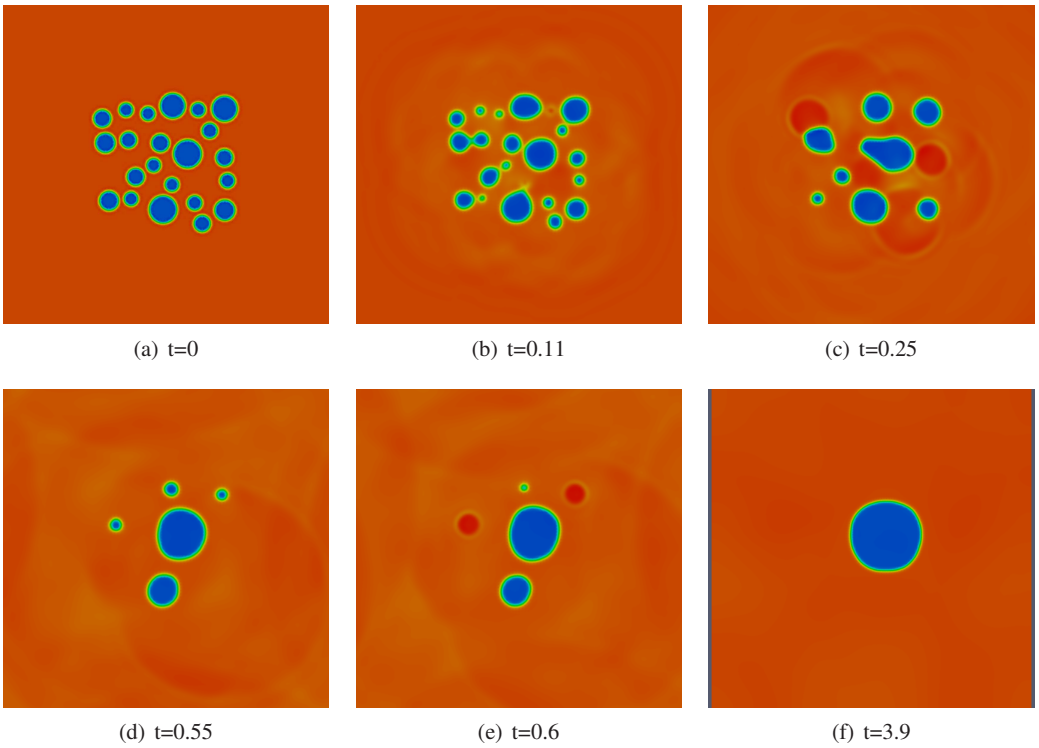

(a) t=0 (b) t=0.11 (c) t=0.25

(d) t=0.55 (e) t=0.6 (f) t=3.9

Figure 6. Density distribution: The density varies between 0.3 (blue) and 1.8 (red). At $t = 0.11,\ 0.25,\ 0.32$, bubbles merge collapse. At $t = 0.55$ the smaller bubbles shrink and the biggest bubble grows. At $t = 0.6$ the two smallest bubble collapse and emit a shock waves. At $t = 3.9$ the material seems to be in an equilibrium state.

Skipping first all terms on the right hand side and neglecting the indices we obtain with $\mathbf{u} = (\rho, m = \rho v)^T$ the first order conservation law

$$\begin{pmatrix} \rho \\ m \end{pmatrix}_t + \mathbf{f}_\alpha \begin{pmatrix} \rho \\ m \end{pmatrix}_x = 0 \Leftrightarrow \mathbf{u}_t + \mathbf{f}_\alpha(\mathbf{u})_x = 0. \tag{44}$$

Let us assume that $\alpha > 0$ is chosen such that $p'_\alpha > 0$ holds and (44) becomes hyperbolic in $\mathcal{U}_\alpha$. Moreover for

$$W_\alpha(\rho) = \frac{\alpha}{2}\rho^2 + W(\rho) \tag{45}$$

the pair (η_α, q_α) given by

$$\eta_\alpha(\rho, m) = W_\alpha(\rho) + \frac{m^2}{2\rho}, \quad q_\alpha(\rho, m) = \frac{m}{\rho}\Big(\eta_\alpha(\rho, m) + p_\alpha(\rho)\Big)$$

is an entropy-entropy flux pair for (44), i.e. we have $(\nabla\eta_\alpha(\mathbf{u}))^T D\mathbf{f}_\alpha(\mathbf{u}) = (\nabla q_\alpha(\mathbf{u}))^T$ for $\mathbf{u} \in \mathcal{U}_\alpha$. Note that (2) and (45) imply $p'_\alpha = \rho W''_\alpha$, such that η_α is convex on the convex state space $\mathcal{U}_\alpha$. As a consequence the mapping $\mathbf{u} \mapsto \mathbf{w}(\mathbf{u})$ from $\mathcal{U}_\alpha$ to $\mathcal{W}_\alpha := \mathbf{w}(\mathcal{U}_\alpha)$ with

$$\mathbf{w}(\mathbf{u}) = (w_1(\mathbf{u}), w_2(\mathbf{u}))^T = \nabla\eta_\alpha(\mathbf{u})^T = \left(W'_\alpha(\rho) - \frac{m^2}{2\rho^2}, \frac{m}{\rho}\right)^T = \left(W'_\alpha(\rho) - \frac{v^2}{2}, v\right)^T$$

is one-to-one. With an appropriate flux function $\mathbf{g}_\alpha = \mathbf{g}_\alpha(\mathbf{w})$ the system (44) can then be rewritten equivalently in terms of the entropy variable $\mathbf{w}$, that is

$$\mathbf{u}(\mathbf{w})_t + \mathbf{g}_\alpha(\mathbf{w})_x = 0. \tag{46}$$

Furthermore the flux $\mathbf{g}_\alpha$ can be represented as the gradient of the potential function (cf. [37])

$$\psi_\alpha(\mathbf{w}) = \mathbf{w} \cdot \mathbf{g}_\alpha(\mathbf{w}) - q_\alpha(\mathbf{u}(\mathbf{w})). \tag{47}$$

In our case we compute

$$\psi_\alpha(\mathbf{w}) = w_2 p_\alpha(\rho(\mathbf{w})). \tag{48}$$

Our numerical scheme relies on so-called entropy-conservative finite difference schemes which have been originally introduced by Tadmor in [37]. In particular we rely on the constructions in the more recent review paper [38]. Let a uniform mesh with cells

$$I_j = (x_{j-\frac{1}{2}}, x_{j+\frac{1}{2}}),\ x_{j+\frac{1}{2}} = \left(j + \frac{1}{2}\right) h,\ j \in \mathbb{Z},$$

and mesh width $h = x_{j+\frac{1}{2}} - x_{j-\frac{1}{2}}$ be given. Now let a numerical flux function $\mathbf{g}^* : \mathcal{W}_\alpha \times \mathcal{W}_\alpha \to \mathbb{R}^2$ with $\mathbf{g}^*(\mathbf{w}, \mathbf{w}) = \mathbf{g}(\mathbf{w})$ for $\mathbf{w} \in \mathcal{W}_\alpha$ be given. Consider a semi-discrete finite volume scheme for (44) which takes for $t \in (0, T)$ and $j \in \mathbb{Z}$ the form

$$\begin{pmatrix} \rho'_j(t) \\ m'_j(t) \end{pmatrix} = -\frac{1}{h}\begin{pmatrix} g^*_{j+\frac{1}{2},1}(t) - g^*_{j-\frac{1}{2},1}(t) \\ g^*_{j+\frac{1}{2},2}(t) - g^*_{j-\frac{1}{2},2}(t) \end{pmatrix} \Leftrightarrow \mathbf{u}'_j(t) = -\frac{1}{h}\left(\mathbf{g}^*_{j+\frac{1}{2}}(t) - \mathbf{g}^*_{j-\frac{1}{2}}(t)\right), \tag{49}$$

such that $\mathbf{g}^*_{j+\frac{1}{2}}(t) = \mathbf{g}^*(\mathbf{w}_j(t), \mathbf{w}_{j+1}(t))$. The following result can be found in [38, Theorem 3.1].

Theorem 5.1. Consider the scheme (49) and assume that

$$(\mathbf{w}_{j+1}(t) - \mathbf{w}_j(t)) \cdot \mathbf{g}^*(\mathbf{w}_j(t), \mathbf{w}_{j+1}(t)) = \psi_\alpha(\mathbf{w}_{j+1}(t)) - \psi_\alpha(\mathbf{w}_{j-1}(t)) \tag{50}$$

is valid for $t \in (0, T)$ and $j \in \mathbb{Z}$.

Then and only then the numerical flux $\mathbf{g}^*$ is *entropy-conservative*, i.e. there is a scalar function

$Q^* = Q^*(\mathbf{w}, \mathbf{z})$ such that $Q(\mathbf{w}, \mathbf{w}) = q_\alpha(\mathbf{u}(\mathbf{w}))$ and

$$\eta_\alpha(\mathbf{u}_j(t))' = -\frac{1}{h}\Big(Q^*(\mathbf{w}_j(t), \mathbf{w}_{j+1}(t)) - Q^*(\mathbf{w}_{j-1}(t), \mathbf{w}_j(t))\Big)$$

hold for all $\mathbf{w}, \mathbf{z} \in \mathcal{W}_\alpha$, $t \in (0,T)$ and $j \in \mathbb{Z}$.

For the systems' case the choice of an entropy-conservative numerical flux is not unique. Let $\{\mathbf{r}^1, \mathbf{r}^2\}, \{\mathbf{l}^1, \mathbf{l}^2\}$ be sets of linear independent vectors in $\mathbb{R}^2$ such that $\mathbf{r}^k \cdot \mathbf{l}^l = \delta_{kl}$. Then we get for $\overline{\mathbf{wz}} := \mathbf{w} + \big(\mathbf{l}^1 \cdot (\mathbf{z} - \mathbf{w})\big)\mathbf{r}^1$:

$$\overline{\mathbf{wz}} + \big(\mathbf{l}^2 \cdot (\mathbf{z} - \mathbf{w})\big)\mathbf{r}^2 = \mathbf{w} + \big(\mathbf{l}^1 \cdot (\mathbf{z} - \mathbf{w})\big)\mathbf{r}^1 + \big(\mathbf{l}^2 \cdot (\mathbf{z} - \mathbf{w})\big)\mathbf{r}^2 = \mathbf{z}. \tag{51}$$

In other words a polygonal path connecting $\mathbf{w}$ and $\mathbf{z}$. In [38, Theorem 6.1] it is shown that any numerical flux of the form

$$\mathbf{g}^*(\mathbf{w}, \mathbf{z}) = \frac{\psi_\alpha\left(\overline{\mathbf{wz}}\right) - \psi_\alpha\left(\mathbf{w}\right)}{\mathbf{l}^1 \cdot (\mathbf{z} - \mathbf{w})}\mathbf{l}^1 + \frac{\psi_\alpha\left(\mathbf{z}\right) - \psi_\alpha\left(\overline{\mathbf{wz}}\right)}{\mathbf{l}^2 \cdot (\mathbf{z} - \mathbf{w})}\mathbf{l}^2 \tag{52}$$

is entropy conservative (and consistent with $\mathbf{g}_\alpha$).
With these preparations we can now present the scheme for the relaxed NSK system (43).

Definition 5.2 (Relaxed Scheme). We set

$$\mathbf{r}^1 = (1,0)^T,\ \mathbf{r}^2 = (0,1),\ \mathbf{l}^1 = (1,0)^T,\ \mathbf{l}^2 = (0,1)^T. \tag{53}$$

We compute for $\mathbf{g}^*(\mathbf{w}, \mathbf{z}) = (g_1^*(\mathbf{w}, \mathbf{z}), g_2^*(\mathbf{w}, \mathbf{z}))^T$

$$\begin{aligned} g_1^*(\mathbf{w}, \mathbf{z}) &= \begin{cases} \frac{w_2 p_\alpha(\rho(\overline{\mathbf{wz}})) - w_2 p_\alpha(\rho(\mathbf{w}))}{z_1 - w_1} & : \quad w_1 \neq z_1, \\ \rho(\mathbf{w}) \cdot w_2 & : \quad w_1 = z_1. \end{cases} \\ g_2^*(\mathbf{w}, \mathbf{z}) &= \begin{cases} \frac{z_2 p_\alpha(\rho(\mathbf{z})) - w_2 p_\alpha(\rho(\overline{\mathbf{wz}}))}{z_2 - w_2} & : \quad w_2 \neq z_2, \\ \rho(\mathbf{z}) * z_2 + p_\alpha(\rho(\mathbf{z})) & : \quad w_2 = z_2. \end{cases} \end{aligned} \tag{54}$$

For $\mathbf{w}, \mathbf{z} \in \mathcal{W}_\alpha$ let

$$h^*(\mathbf{w}, \mathbf{z}) = \begin{cases} \frac{p_\alpha(\rho(\overline{\mathbf{wz}})) - p_\alpha(\rho(\mathbf{w}))}{z_1 - w_1} & : \quad w_1 \neq z_1. \\ \rho(\mathbf{w}) & : \quad w_1 = z_1. \end{cases} \tag{55}$$

For $j \in \mathbb{Z}$ a solution $(\rho_j, m_j, c_j) : [0,T) \to \mathcal{U} \times \mathbb{R}$ of the initial value problem

$$\begin{aligned} \begin{pmatrix} \rho_j'(t) \\ m_j'(t) \end{pmatrix} &= -\frac{1}{h}\begin{pmatrix} g^*_{j+\frac{1}{2},1}(t) - g^*_{j-\frac{1}{2},1}(t) \\ g^*_{j+\frac{1}{2},2}(t) - g^*_{j-\frac{1}{2},2}(t) \end{pmatrix} \\ &\quad + \frac{\varepsilon\beta}{h^2}\begin{pmatrix} 0 \\ v_{j+1}(t) - 2v_j(t) + v_{j-1}(t) \end{pmatrix} \\ &\quad + \frac{\alpha}{h}\begin{pmatrix} 0 \\ h^*(\mathbf{w}_j(t), \mathbf{w}_{j+1}(t))\big(c_{j+1}(t) - c_j(t)\big) \end{pmatrix}, \qquad (t \in (0,T)) \\ -\frac{\gamma\varepsilon^2}{h^2}\left(c_{j+1}(t) - 2c_j(t) + c_{j-1}(t)\right) &= \alpha(\rho_j(t) - c_j(t)) \end{aligned} \tag{56}$$

and

$$\rho_j(0) = \int_{I_j} \rho_0(x)\,dx, \quad m_j(0) = \int_{I_j} \rho_0(x)v_0(x)\,dx \tag{57}$$

is called a *relaxed approximation* of (43).

We can now present the main result of this section.

Theorem 5.3 (Discrete Energy Inequality)**.** Let $\rho_0 v_0^2, \rho_0^2, W(\rho_0) \in L^1(\mathbb{R}) \cap L^\infty(\mathbb{R})$. For $j \in \mathbb{Z}$ let $(\rho_j, m_j, c_j) : [0,T) \to \mathcal{U}_\alpha \times \mathbb{R}$ be a relaxed approximation defined by (56),(57).
Then we have for each $t \in [0,T)$ the discrete energy inequality

$$\sum_{j\in\mathbb{Z}} \left(\frac{(m_j(t))^2}{2\rho_j(t)} + W(\rho_j) + \frac{\alpha}{2}\left((\rho_j(t) - c_j(t))^2 + \frac{\gamma\varepsilon^2}{2\Delta x^2}\left(c_{j+1}(t) - c_j(t)\right)^2\right) \right) \leq \mathcal{E}^{\varepsilon,\alpha}[\rho_0, v_0]. \tag{58}$$

Proof

Consider the the numerical flux $h^*(\mathbf{w}, \mathbf{z})$. One can easily see that

$$h^*(\mathbf{w}, \mathbf{z})w_2 = g_1^*(\mathbf{w}, \mathbf{z}). \tag{59}$$

Now we consider the scheme (56) and multiply the two evolution equations by $\mathbf{w}_j(t)$. Arguing as in [38, pp. 463] we obtain from Theorem 5.1 functions $Q^* = Q^*(\mathbf{w}, \mathbf{z})$ such that

$$\begin{aligned}
&\eta_\alpha(\mathbf{u}_j(t))' + \frac{1}{h}\left(Q^*(\mathbf{w}_j(t), \mathbf{w}_{j+1}(t) - Q^*(\mathbf{w}_{j-1}(t), \mathbf{w}_j(t))\right) \\
&= \quad + \frac{\varepsilon\beta}{h^2}\begin{pmatrix} 0 \\ v_{j+1}(t) - 2v_j(t) + v_{j+1}(t) \end{pmatrix} \cdot \mathbf{w}_j(t) \\
&\qquad + \frac{\alpha}{h}\begin{pmatrix} 0 \\ h^*(\mathbf{w}_j(t), \mathbf{w}_{j+1}(t))\big(c_{j+1}(t) - c_j(t)\big) \end{pmatrix} \cdot \mathbf{w}_j(t) \\
&= \quad + \frac{\varepsilon\beta}{h^2}\begin{pmatrix} 0 \\ v_{j+1}(t) - 2v_j(t) + v_{j+1}(t) \end{pmatrix} \cdot \mathbf{w}_j(t) \\
&\qquad + \frac{\alpha}{h}\begin{pmatrix} 0 \\ g_1^*(\mathbf{w}_j(t), \mathbf{w}_{j+1}(t))\big(c_{j+1}(t) - c_j(t)\big) \end{pmatrix}.
\end{aligned}$$

The last line follows from (59) above.
In the next step we sum up with respect to $j \in \mathbb{Z}$ and obtain with summation by parts

$$\begin{aligned}
\sum_{j\in\mathbb{Z}} \eta_\alpha(\mathbf{u}_j(t))' &\leq \frac{\alpha}{h}\sum_{j\in\mathbb{Z}} g^*_{j+\frac{1}{2},1}(t)(c_{j+1}(t) - c_j(t)) \\
&= -\frac{\alpha}{h}\sum_{j\in\mathbb{Z}} \left(g^*_{j+\frac{1}{2},1}(t) - g^*_{j-\frac{1}{2},1}(t)\right) c_j(t) \\
&= \alpha\sum_{j\in\mathbb{Z}} \rho_j'(t)c_j(t).
\end{aligned} \tag{60}$$

For the last equality we used the evolution equation for ρ_j in (56). We turn to the equation for c_j which we multiply with c_j' and add up with respect to $j \in \mathbb{Z}$. This gives again using summation by

parts and shifting indices

$$\frac{\gamma\varepsilon^2}{2\Delta x^2}\sum_{j\in\mathbb{Z}}\left(\Big(c_{j+1}(t)-c_j(t)\Big)^2\right)' = \frac{\alpha}{2}\sum_{j\in\mathbb{Z}}\Big(2\rho_j(t)c_j'(t)-((c_j(t))^2)'\Big). \tag{61}$$

Adding up inequality (60) and equation (61) we get the result (58) from the definition (47) of η_α, the definition of (45) of W_α, and the definition of the initial values in (57). □

We illustrate the behaviour of the finite volume scheme (56),(57) by the following example. Let us state that we consider the DG approach from section 3 to be more efficient. However we are able to verify a statement that corresponds to Theorem 5.3.

Example 5.4. (Numerical Confirmation) We set with $d = 1$ the initial conditions

$$\rho_0(x) = \begin{cases} 1.8, & x \in (0.15, 0.55) \cup (0.665, 0.735) \\ .3, & \text{else} \end{cases} \qquad v_0(x) = 0. \tag{62}$$

and $\alpha = 100$, $h = 0.005$, $\varepsilon = 0.1$, $\gamma = .001$. We use forward Euler time stepping and obtain a stable numerical scheme for our choice of ε. Figure 8 displays the monotone decay of the total energy for

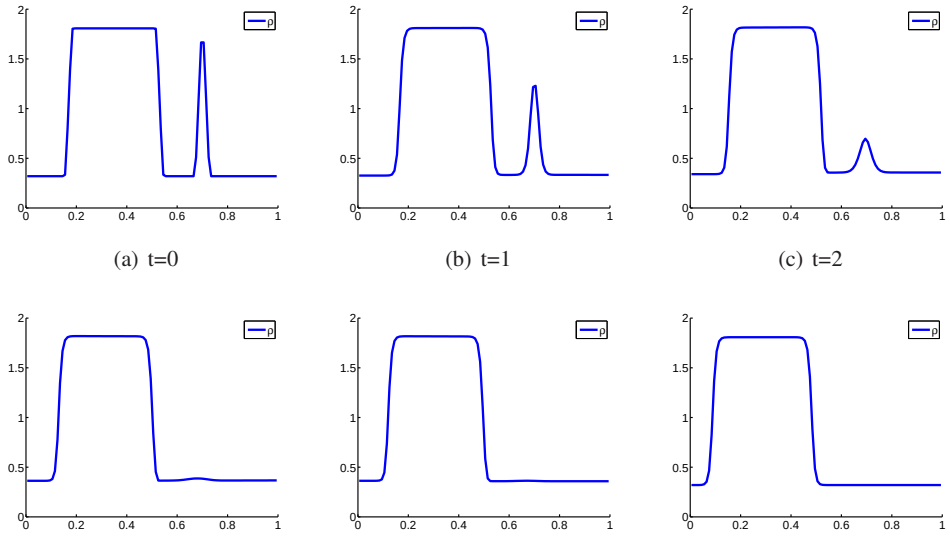

(a) t=0 (b) t=1 (c) t=2

(d) t=3 (e) t=3.5 (f) t=20

Figure 7. Time evolution of the density for a setting with the entropy conserving scheme for the relaxed NSK system

the numerical scheme 56 as shown in theorem 5.3.

REFERENCES

1. G. L. Aki, W. Dreyer, J. Giesselmann, and C. Kraus. A quasi-incompressible diffuse interface model with phase transition. *Mathematical Models and Methods in Applied Sciences*, 24(5):827–861, 2014.
2. D. M. Anderson, G. B. McFadden, and A. A. Wheeler. Diffuse-interface methods in fluid mechanics. *Annual Review of Fluid Mechanics*, 30(1):139–165, 1998.

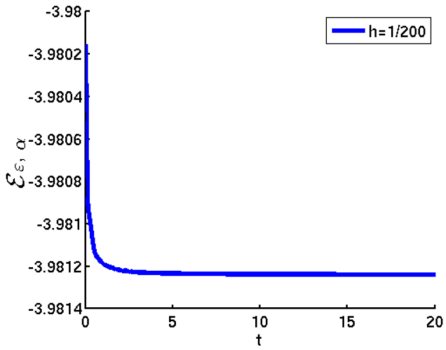

Figure 8. Evolution of the energy (20) for discretization 56 of the relaxed NSK system.

3. F. Bassi and S. Rebay. A high-order accurate discontinuous finite element method for the numerical solution of the compressible Navier-Stokes equations. *Journal of Computational Physics*, 131(2):267 – 279, 1997.
4. S. Benzoni-Gavage. Nonuniqueness of phase transitions near the Maxwell line. *Proc. Amer. Math. Soc.*, 127(4):1183–1190, 1999.
5. T. Blesgen. A generalization of the Navier-Stokes equations to two-phase flows. *J. Phys. D: Appl. Phys.*, 32:1119–1123, 1999.
6. M. Braack and A. Prohl. Stable discretization of a diffuse interface model for liquid-vapor flows with surface tension. *ESAIM Math. Model. Numer. Anal.*, 47(2):401–420, 2013.
7. D. Bresch, B. Desjardins, and C.-K. Lin. On some compressible fluid models: Korteweg, lubrication, and shallow water systems. *Comm. Partial Differential Equations*, 28(3-4):843–868, 2003.
8. F. Charve. Convergence of a low order non-local Navier-Stokes-Korteweg system: the order-parameter model. *http://arxiv.org/abs/1302.2617*, February 2013.
9. Frédéric Charve. Local in time results for local and non-local capillary Navier–Stokes systems with large data. *Journal of Differential Equations*, 256(7):2152–2193, 2014.
10. B. Cockburn and C.-W. Shu. TVB Runge-Kutta local projection discontinuous Galerkin finite element method for conservation laws. II. General framework. *Math. Comp.*, 52(186):411–435, 1989.
11. B. Cockburn, S. Y. Lin, and C.-W. Shu. TVB Runge-Kutta local projection discontinuous Galerkin finite element method for conservation laws. III. One-dimensional systems. *J. Comput. Phys.*, 84(1):90–113, 1989.
12. B. Cockburn, S. Hou, and C.-W. Shu. The Runge-Kutta local projection discontinuous Galerkin finite element method for conservation laws. IV. The multidimensional case. *Math. Comp.*, 54(190):545–581, 1990.
13. F. Coquel, D. Diehl, C. Merkle, and C. Rohde. Sharp and diffuse interface methods for phase transition problems in liquid-vapour flows. In *Numerical methods for hyperbolic and kinetic problems*, volume 7, pages 239–270. Eur. Math. Soc., Zürich, 2005.
14. A. Corli and C. Rohde. Singular limits for a parabolic-elliptic regularization of scalar conservation laws. *J. Differential Eq.*, 253(5):1399–1421, 2012.
15. G. Dal Maso, P. G. Lefloch, and F. Murat. Definition and weak stability of nonconservative products. *Journal de mathématiques pures et appliquées*, 74(6):483–548, 1995.
16. D. Diehl. *Higher order schemes for simulation of compressible liquid-vapor flows with phase change*. PhD thesis, Albert-Ludwigs-Universität Freiburg, 2007.
17. W. Dreyer, J. Giesselmann, C. Kraus, and C. Rohde. Asymptotic analysis for Korteweg models. *Interfaces Free Bound.*, 14(1):105–143, 2012.
18. J.E. Dunn and J. Serrin. On the thermomechanics of interstitial working. *Archive for Rational Mechanics and Analysis*, 88(2):95–133, 1985.
19. P. Engel, A. Viorel, and C. Rohde. A low-order approximation for viscous-capillary phase transition dynamics. *Port. Math.*, 70(4):319–344, 2014.
20. J. Giesselmann. A relative entropy approach to convergence of a low order approximation to a nonlinear elasticity model with viscosity and capillarity. *SIAM Journal on Mathematical Analysis*, 46(5):3518–3539, 2014.
21. J. Giesselmann, C. Lattanzio, A. Tzavaras. Relative entropy for Hamiltonian flows *In preparation*
22. J. Giesselmann, C. Makridakis, and T. Pryer. Energy consistent DG methods for the Navier-Stokes-Korteweg system. *Mathematics of Computation*, 83:2071 – 2099, 2014.
23. P. Glaister. An approximate linearised Riemann solver for the Euler equations for real gases. *Journal of Computational Physics*, 74(2):382 – 408, 1988.
24. J. Haink and C. Rohde. Local discontinuous-Galerkin schemes for model problems in phase transition theory. *Commun. Comput. Phys.*, 4(4):860–893, 2008.
25. H. Hattori and D. Li. Solutions for two-dimensional system for materials of Korteweg type. *SIAM J. Math. Anal.*, 25(1):85–98, 1994.
26. K. Hermsdörfer, C. Kraus, and D. Kröner. Interface conditions for limits of the Navier-Stokes-Korteweg model. *Interfaces Free Bound.*, 13(2):239–254, 2011.
27. D. Jamet, O. Lebaigue, N. Coutris, and J.M. Delhaye. The second gradient method for the direct numerical simulation of liquid–vapor flows with phase change. *Journal of Computational Physics*, 169(2):624–651, 2001.

28. D.J. Korteweg. Sur la forme que prennent les équations du mouvement des fluides si l'on tient compte des forces capillaires causées par des variations de densitè considérables mais continues et sur la thèorie de la capillarité dans l'hypothèse d'une variation continue de la densité. *Archives Néerlandaises de Sciences Exactes et Naturelles*, 2(6):1–24, 1901.
29. M. Kotschote. Strong solutions for a compressible fluid model of Korteweg type. *Annales de l'Institut Henri Poincare (C) Non Linear Analysis*, 25(4):679–696, 2008.
30. D. Kröner. *Numerical schemes for conservation laws*. Wiley-Teubner Series Advances in Numerical Mathematics. John Wiley & Sons Ltd., Chichester, 1997.
31. B. Rivière. Discontinuous Galerkin Methods for solving elliptic and Parabolic Equations: Theory and Implementation. *Frontiers in Applied Mathematics. Society for Industrial and Applied Mathematics*, 2008.
32. P.L. Roe. Approximate Riemann solvers, parameter vectors, and difference schemes. *Journal of Computational Physics*, 43(2):357–372, 1981.
33. C. Rohde. On local and non-local Navier-Stokes-Korteweg systems for liquid-vapour phase transitions. *ZAMM Z. Angew. Math. Mech.*, 85(12):839–857, 2005.
34. C. Rohde. A local and low-order Navier-Stokes-Korteweg system. In *Nonlinear partial differential equations and hyperbolic wave phenomena*, volume 526, pages 315–337. Amer. Math. Soc., 2010.
35. C.-W. Shu and S. Osher. Efficient implementation of essentially nonoscillatory shock-capturing schemes. *J. Comput. Phys.*, 77(2):439–471, 1988.
36. M. Solci. *A Variational Model for phase separation*. PhD thesis, Scuola Normale Superiore Pisa, 2002.
37. E. Tadmor. Numerical viscosity and the entropy condition for conservative difference schemes. *Math. Comp.*, 43(168):369–381, 1984.
38. E. Tadmor. Entropy stability theory for difference approximations of nonlinear conservation laws and related time-dependent problems. *Acta Numer.*, 12:451–512, 2003.
39. L. Tian, Y. Xu, J. G. M. Kuerten and J. J. W. Van der Vegt. A local discontinuous Galerkin method for the propagation of phase transition in solids and fluids. *J. Sci. Comput.*, 59(3):688–720, 2014.
40. G. Witterstein. Phase change flows with mass exchange. *Adv. Math. Sci. Appl.*, 21(2):559–611, 2011.

Jochen Neusser
Pfaffenwaldring 57
70569 Stuttgart
Germany
E-Mail: jochen.neusser@mathematik.uni-stuttgart.de
WWW: http://www.ians.uni-stuttgart.de/am/mitarbeiter/neusser/

Christian Rohde
Pfaffenwaldring 57
70569 Stuttgart
Germany
E-Mail: crohde@mathematik.uni-stuttgart.de
WWW: http://www.mathematik.uni-stuttgart.de/fak8/ians/lehrstuhl/LstAngMath/mitarbeiter/rohde

Veronika Schleper
Pfaffenwaldring 57
70569 Stuttgart
Germany
E-Mail: veronika.schleper@mathematik.uni-stuttgart.de
WWW: http://www.ians.uni-stuttgart.de/am/mitarbeiter/schleper/

Erschienene Preprints ab Nummer 2012-001

Komplette Liste: `http://www.mathematik.uni-stuttgart.de/preprints`

2014-021 *Neusser, J.; Rohde, C.; Schleper, V.:* Relaxed Navier-Stokes-Korteweg Equations for Compressible Two-Phase Flow with Phase Transition

2014-020 *Kabil, B.; Rohde, C.:* Persistence of undercompressive phase boundaries for isothermal Euler equations including configurational forces and surface tension

2014-019 *Bilyk, D.; Markhasin, L.:* BMO and exponential Orlicz space estimates of the discrepancy function in arbitrary dimension

2014-018 *Schmid, J.:* Well-posedness of non-autonomous linear evolution equations for generators whose commutators are scalar

2014-017 *Margolis, L.:* A Sylow theorem for the integral group ring of $PSL(2,q)$

2014-016 *Rybak, I.; Magiera, J.; Helmig, R.; Rohde, C.:* Multirate time integration for coupled saturated/unsaturated porous medium and free flow systems

2014-015 *Gaspoz, F.D.; Heine, C.-J.; Siebert, K.G.:* Optimal Grading of the Newest Vertex Bisection and H^1-Stability of the L_2-Projection

2014-014 *Kohler, M.; Krzyżak, A.; Walk, H.:* Nonparametric recursive quantile estimation

2014-013 *Kohler, M.; Krzyżak, A.; Tent, R.; Walk, H.:* Nonparametric quantile estimation using importance sampling

2014-012 *Györfi, L.; Ottucsák, G.; Walk, H.:* The growth optimal investment strategy is secure, too.

2014-011 *Györfi, L.; Walk, H.:* Strongly consistent detection for nonparametric hypotheses

2014-010 *Köster, I.:* Finite Groups with Sylow numbers $\{q^x, a, b\}$

2014-009 *Kahnert, D.:* Hausdorff Dimension of Rings

2014-008 *Steinwart, I.:* Measuring the Capacity of Sets of Functions in the Analysis of ERM

2014-007 *Steinwart, I.:* Convergence Types and Rates in Generic Karhunen-Loève Expansions with Applications to Sample Path Properties

2014-006 *Steinwart, I.; Pasin, C.; Williamson, R.; Zhang, S.:* Elicitation and Identification of Properties

2014-005 *Schmid, J.; Griesemer, M.:* Integration of Non-Autonomous Linear Evolution Equations

2014-004 *Markhasin, L.:* L_2- and $S^r_{p,q}B$-discrepancy of (order 2) digital nets

2014-003 *Markhasin, L.:* Discrepancy and integration in function spaces with dominating mixed smoothness

2014-002 *Eberts, M.; Steinwart, I.:* Optimal Learning Rates for Localized SVMs

2014-001 *Giesselmann, J.:* A relative entropy approach to convergence of a low order approximation to a nonlinear elasticity model with viscosity and capillarity

2013-016 *Steinwart, I.:* Fully Adaptive Density-Based Clustering

2013-015 *Steinwart, I.:* Some Remarks on the Statistical Analysis of SVMs and Related Methods

2013-014 *Rohde, C.; Zeiler, C.:* A Relaxation Riemann Solver for Compressible Two-Phase Flow with Phase Transition and Surface Tension

2013-013 *Moroianu, A.; Semmelmann, U.:* Generalized Killling spinors on Einstein manifolds

2013-012 *Moroianu, A.; Semmelmann, U.:* Generalized Killing Spinors on Spheres

2013-011 *Kohls, K; Rösch, A.; Siebert, K.G.:* Convergence of Adaptive Finite Elements for Control Constrained Optimal Control Problems

2013-010 *Corli, A.; Rohde, C.; Schleper, V.:* Parabolic Approximations of Diffusive-Dispersive Equations

2013-009 *Nava-Yazdani, E.; Polthier, K.:* De Casteljau's Algorithm on Manifolds

2013-008 *Bächle, A.; Margolis, L.:* Rational conjugacy of torsion units in integral group rings of non-solvable groups

2013-007 *Knarr, N.; Stroppel, M.J.:* Heisenberg groups over composition algebras

2013-006 *Knarr, N.; Stroppel, M.J.:* Heisenberg groups, semifields, and translation planes

2013-005 *Eck, C.; Kutter, M.; Sändig, A.-M.; Rohde, C.:* A Two Scale Model for Liquid Phase Epitaxy with Elasticity: An Iterative Procedure

2013-004 *Griesemer, M.; Wellig, D.:* The Strong-Coupling Polaron in Electromagnetic Fields

2013-003 *Kabil, B.; Rohde, C.:* The Influence of Surface Tension and Configurational Forces on the Stability of Liquid-Vapor Interfaces

2013-002 *Devroye, L.; Ferrario, P.G.; Györfi, L.; Walk, H.:* Strong universal consistent estimate of the minimum mean squared error

2013-001 *Kohls, K.; Rösch, A.; Siebert, K.G.:* A Posteriori Error Analysis of Optimal Control Problems with Control Constraints

2012-013 *Diaz Ramos, J.C.; Dominguez Vázquez, M.; Kollross, A.:* Polar actions on complex hyperbolic spaces

2012-012 *Moroianu; A.; Semmelmann, U.:* Weakly complex homogeneous spaces

2012-011 *Moroianu; A.; Semmelmann, U.:* Invariant four-forms and symmetric pairs

2012-010 *Hamilton, M.J.D.:* The closure of the symplectic cone of elliptic surfaces

2012-009 *Hamilton, M.J.D.:* Iterated fibre sums of algebraic Lefschetz fibrations

2012-008 *Hamilton, M.J.D.:* The minimal genus problem for elliptic surfaces

2012-007 *Ferrario, P.:* Partitioning estimation of local variance based on nearest neighbors under censoring

2012-006 *Stroppel, M.:* Buttons, Holes and Loops of String: Lacing the Doily

2012-005 *Hantsch, F.:* Existence of Minimizers in Restricted Hartree-Fock Theory

2012-004 *Grundhöfer, T.; Stroppel, M.; Van Maldeghem, H.:* Unitals admitting all translations

2012-003 *Hamilton, M.J.D.:* Representing homology classes by symplectic surfaces

2012-002 *Hamilton, M.J.D.:* On certain exotic 4-manifolds of Akhmedov and Park

2012-001 *Jentsch, T.:* Parallel submanifolds of the real 2-Grassmannian